Inorg. Chem. **2004**, *43*, 7324–7338

Nonoxovanadium(IV) and Oxovanadium(V) Complexes with Mixed O, X, O-Donor Ligands (X = S, Se, P, or PO)

Tapan K. Paine, Thomas Weyhermüller, Leonardo D. Slep, Frank Neese, Eckhard Bill, Eberhard Bothe, Karl Wieghardt, and Phalguni Chaudhuri*

Max-Planck-Institut für Bioanorganische Chemie, Stiftstrasse 34-36, D-45470 Mülheim an der Ruhr, Germany

Received April 5, 2004

Ligating properties of four potentially tridentate bisphenol ligands containing [O, X, O] donor atoms (X = S **1**, Se **2**, P **3**, or P=O **4**) toward the vanadium ions in +IV or +V oxidation states have been studied. Each ligand with different heterodonor atoms yields as expected nonoxovanadium(IV) complexes, $V^{IV}L_2$, whose structures have been determined by X-ray diffraction methods as having six-coordinate V^{IV}, VO_4X_2, core. Compounds **1**–**4** have also been studied with electrochemical methods, variable-temperature (2–295 K) magnetic susceptibility measurements, X-band electron paramagnetic resonanace (EPR) (2–60 K) spectroscopy, and magnetic circular dichroism (MCD) (5 K) measurements. Electrochemical results suggest metal-centered oxidations to V^{V} (i.e., no formation of phenoxyl radicals from the coordinated phenolates). A combination of density functional theory calculations and experimental EPR investigations indicates a dramatic effect of the heteroatoms on the electronic structure of **1**–**4** with consequent reordering of the energy levels; **1** and **3** possess a trigonal ground state $(d_{z^2})^1$, but **4** with the phosphoryl oxygen as the heterodonor atom in contrast exhibits a tetragonal ground state, $(d_{xy})^1$. On the basis of the intense electronic transitions in absorption spectra, all electronic transitions observed for **4** have been assigned to ligand-to-metal charge-transfer transitions, which have been confirmed by preliminary resonance Raman measurements and C/D ratios obtained from low-temperature MCD spectroscopy. Moreover, diamagnetic complexes **5** and **6** containing mononuclear and dinuclear oxovanadium(V) units have also been synthesized and structurally and spectroscopically (^{51}V NMR) characterized.

Introduction

This work stems from our continuing interest in the coordination chemistry of phenol-containing ligands,[1] whose investigations were fueled mainly by the growing awareness of the existence of tyrosyl (i.e., phenoxyl) radicals[2] in a rapidly increasing number of oxygen-dependent metalloenzymes. There are several intriguing features associated with ligands containing two phenolate donor atoms. First, these ligands with good π-donor atoms are expected to stabilize higher oxidation states with highly covalent M−O (phenolate) bonds. There is now substantial evidence that Mn(III)−phenolate species are susceptible to air-oxidation to stable Mn(IV) species.[1f,i,3] A second general reason to study bisphenol ligands is that they may produce, in the presence of air, phenoxyl radicals to be used as bioinspired radical catalysts for the conversion of different organic substrates.[1a−c,4]

* Author to whom correspondence should be addressed. E-mail: chaudh@mpi-muelheim.mpg.de.

(1) Selected examples: (a) Chaudhuri, P.; Hess, M.; Flörke, U.; Wieghardt, K. *Angew. Chem., Int. Ed.* **1998**, *110*, 2217. (b) Chaudhuri, P.; Hess, M.; Weyhermüller, T.; Wieghardt, K. *Angew. Chem., Int. Ed.* **1999**, *38*, 1095. (c) Chaudhuri, P.; Hess, M.; Müller, J.; Hildenbrand, K.; Bill, E.; Weyhermüller, T.; Wieghardt, K. *J. Am. Chem. Soc.* **1999**, *121*, 9599. (d) Siefert, R.; Weyhermüller, T.; Chaudhuri, P. *J. Chem. Soc., Dalton Trans.* **2000**, 4656. (e) Verani, C. N.; Bothe, E.; Burdinski, D.; Weyhermüller, T.; Flörke, U.; Chaudhuri, P. *Eur. J. Inorg. Chem.* **2001**, 2161. (f) Weyhermüller, T.; Paine, T. K.; Bothe, E.; Bill, E.; Chaudhuri, P. *Inorg. Chim. Acta* **2002**, *337*, 344. (g) Paine, T. K.; Weyhermüller, T.; Wieghardt, K.; Chaudhuri, P. *Inorg. Chem.* **2002**, *41*, 6538. (h) Mukherjee, S.; Weyhermüller, T.; Bothe, E.; Wieghardt, K.; Chaudhuri, P. *Eur. J. Inorg. Chem.* **2003**, 863. (i) Paine, T. K.; Weyhermüller, T.; Bothe, E.; Wieghardt, K.; Chaudhuri, P. *Dalton Trans.* **2003**, 3136. (j) Paine, T. K.; Weyhermüller, T.; Bill, E.; Bothe, E.; Chaudhuri, P. *Eur. J. Inorg. Chem.* **2003**, 4299.

(2) (a) Holm, R. H.; Solomon. E. I., Eds. *Chem. Rev.* **1996**, *96*, 6. (b) *Metal Ions in Biological Systems*; Sigel, H., Sigel, A., Eds.; Marcel Dekker: New York, 1994; Vol. 30. (c) Babcock, G. T.; Espe, M.; Hoganson, C.; Lydakis-Simantiris, N.; McCracken, J.; Shi, W.; Styring, S.; Tommas, C.; Warncke, K. *Acta Chem. Scand.* **1997**, *51*, 533. (d) Fontecave, M. M.; Pierre, J. J. *Bull. Soc. Chim. Fr.* **1996**, *133*, 653. (e) Goldberg, D. P.; Lippard, S. J. *Adv. Chem. Ser.* **1995**, *246*, 59. (f) Stubbe, J.; van der Donk, W. A. *Chem. Rev.* **1998**, *98*, 705. (g) Chaudhuri, P.; Wieghardt, K. *Prog. Inorg. Chem.* **2002**, *50*, 151.

10.1021/ic040052f CCC: $27.50
Published on Web 10/20/2004

It is now well established that vanadium occurs in a variety of biological systems[5] (e.g., in amavadin,[6] a compound isolated from the mushroom *Amanita muscaria)*. Amavadin has been shown to contain an eight-coordinate V^{5+} ion[7] without oxo ligands, a so-called "bare" or nonoxovanadium species, that is still scarce[8] in oxophilic oxidation states +IV and +V of vanadium, whose complexes containing VO^{2+}, VO^{3+}, or VO_2^+ groups still predominate.[9] Nonoxovanadium centers have also been reported for the cofactor in vanadium nitrogenase. Vanadium-dependent non-heme haloperoxidases are found in a variety of marine algae and lichens and catalyze the formation of a number of halogenated organic compounds.[10] There are also certain sea squirts or tunicates (polyphenol ascidians) that are able to uptake vanadium(V) from seawater and to store vanadium as V(III) in high concentrations.[11] Moreover, inorganic vanadyl and vanadate, as well as some vanadium(IV) and (V) complexes, are potent insulin mimics and as such may find use as alternatives to insulin in the treatment of diabetes.[12] Vanadium in nature coordinates to O, N, and S donor atoms of the biological ligands. For example, the O functionalities of phenolates from tyrosine residues are present in vanadium-modified transferrin.[13] The diversified roles of vanadium among others in biological systems are primarily responsible for stimulating a recent increasing interest in vanadium coordination chemistry. Although the chemistry of oxovanadium(IV) and (V) complexes is well developed,[9] far less information is available for non-oxo complexes,[8] particularly concerning their electron paramagnetic resonance (EPR) spectroscopic properties. The vanadyl ion ranks among the most stable of diatomic cations and dominates the chemistry of vanadium.

We have been exploring the feasibility of using tridentate bisphenol ligands,[1a,d,f,g,i] which comprise three donor atoms such as [O, X, O], where X = N, S, Se, P, and P=O, to generate novel transition-metal complexes. We felt it would be interesting to examine the effect of attaching heterodonor (X) groups to the two phenolate groups as ligands. Here, we describe four mononuclear octahedral vanadium(IV) complexes, ML_2 **1**−**4**, with the ligands H_2L^S, H_2L^{Se}, H_2L^P, and H_2L^{PO} that are depicted in Chart 1. Our expectation of nonoxovanadium(IV) complexes was confirmed, as is authenticated by structure determinations, the results of which together with the EPR and electrochemical investigations are described herein. Two oxovanadium(V) compounds **5** and **6** will also be described. Nonoxovanadium(IV) complexes of amine-bis(phenolate) [O, N, O] donor ligands have been reported recently by us.[1j] Chart 1 shows the complexes prepared with the ligands and their labels. The sulfur analogue of **6**, $[V^V_2O_2L^S_2(\mu_2\text{-OH})_2]$, has recently been reported.[14]

Chart 1

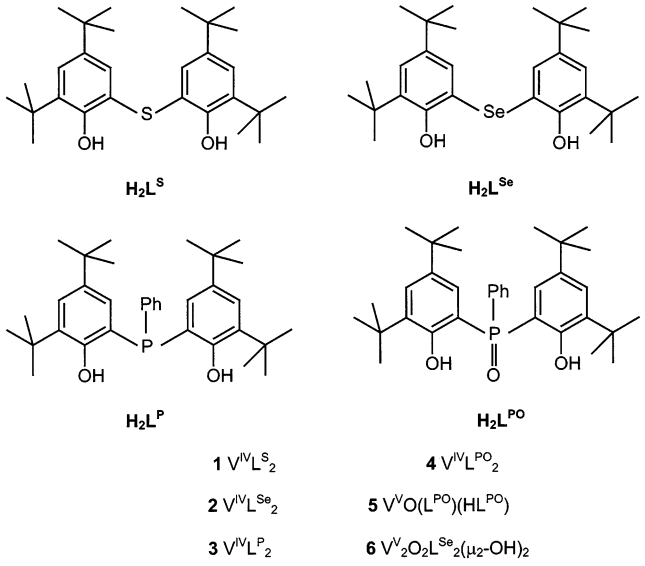

(3) Selected examples: (a) Lynch, M. W.; Hendrickson, D. N.; Fritzgerald, B. J.; Pierpont, C. G. *J. Am. Chem. Soc.* **1984**, *106*, 2041. (b) Hartman, J. H.; Foxman, B. M.; Cooper, S. R. *Inorg. Chem.* **1984**, *23*, 1381. (c) Chandra, S. K.; Basu, P.; Ray, D.; Pal, S.; Chakravorthy, A. *Inorg. Chem.* **1990**, *29*, 2423 and references therein. (d) Mikuriya, M.; Shigematsu, S.; Kawano, K.; Tokii, T.; Oshio, H. *Chem. Lett.* **1990**, 729. (e) Adam, B.; Bill, E.; Bothe, E.; Goerdt, B.; Haselhorst, G.; Hildenbrand, K.; Sokolowski, A.; Steenken, S.; Weyhermüller, T.; Wieghardt, K. *Chem.*−*Eur. J.* **1997**, *3*, 308 and references therein.

(4) (a) Wang, Y.; Stack, T. D. P. *J. Am. Chem. Soc.* **1996**, *118*, 13097. (b) Wang, Y.; DuBois, J. L.; Hedman, B.; Hodgson, K. O.; Stack, T. D. P. *Science* **1998**, *279*, 537. (c) Thomas, F.; Gelbon, G.; Luneau, I. G.; Aman, E. S.; Pierre, J.-L. *Angew. Chem., Int. Ed.* **2002**, *41*, 3047.

(5) (a) Kustin, K.; McLeod, G. C. *Struct. Bonding (Berlin)* **1983**, *53*, 140. (b) Rehder, D. *Angew. Chem., Int. Ed. Engl.* **1991**, *30*, 148. (c) Rehder, D. *Coord. Chem. Rev.* **1999**, *182*, 297. (d) *Vanadium and its Role in Life*; Sigel, H.; Sigel, A.. Eds.; Metal Ions in Biological Systems, Vol. 31; Marcel-Dekker: New York, **1995**. (e) *J. Inorg. Biochem.* **2000**, 80. (A special issue dedicated to biological aspects of vanadium.) (f) *Coord. Chem. Rev.* **2003**, *237* (*1*−*2*). (A special issue: "New Directions in Chemistry and Biological Chemistry of Vanadium")

(6) (a) Bayer, E.; Kneifel, H. *Z. Naturforsch., B: Chem. Sci.* **1972**, *27*, 207. (b) Kneifel, H.; Bayer, E. *J. Am. Chem. Soc.* **1986**, *108*, 1075.

(7) Berry, R. E.; Armstrong, E. M.; Beddoes, R. L.; Collison, D.; Ertok, S. N.; Helliwell, M.; Garner, C. D. *Angew. Chem., Int. Ed.* **1999**, *38*, 795.

(8) (a) Cooper, S. R.; Koh, Y. B.; Raymond, K. N. *J. Am. Chem. Soc.* **1982**, *104*, 5092. (b) Auerbach, U.; Della Vedova, B. P. C.; Wieghardt, K.; Nuber, B.; Weiss, J. *J. Chem. Soc., Chem. Commun.* **1990**, 1004. (c) Kabanas, T. A.; White, A. J. P.; Williams, D. J.; Woollins, J. D. *J. Chem. Soc., Chem. Commun.* **1992**, 17. (d) Neves, A.; Ceccato, A. S.; Vencato, I.; Mascarenhas, Y. P.; Erasmus-Buhr, C. *J. Chem. Soc., Chem. Commun.* **1992**, 652. (e) Kabanos, T. A.; Slawin, A. M. Z.; Williams, D. J.; Woollins, J. D. *J. Chem. Soc., Dalton Trans.* **1992**, 1423. (f) Bruni, S.; Caneschi, A.; Cariatia, F.; Delfs, C.; Dei, A.; Gatteschi, D. *J. Am. Chem. Soc.* **1994**, *116*, 1388. (g) Gergopoulos, V.; Jantzen, S.; Rodewald, D.; Rehder, D. *J. Chem. Soc., Chem. Commun.* **1995**, 377. (h) Klich, P. R.; Daniher, A. D.; Challen, P. R.; McConville, D. B.; Youngs, W. J. *Inorg. Chem.* **1996**, *35*, 347. (i) Farahbakhsh, M.; Schmidt, H.; Rehder, D. *Chem. Commun.* **1998**, 2009. (j) Kang, B.; Wenig, L.; Liu, H.; Wu, D.; Huang, L.; Lu, C.; Cai, J.; Chen, X.; Lu, J. *Inorg. Chem.* **1990**, *29*, 4873. (k) Ludwig, E.; Hefele, H.; Uhlemann, E.; Weller, F.; Kläui, W. *Z. Anorg. Allg. Chem.* **1995**, *621*, 23. (l) Hefele, H.; Ludwig, E.; Uhlemann, E.; Weller, F. *Z. Anorg. Allg. Chem.* **1995**, *621*, 1973. (m) Diamantis, A. A.; Snow, M. R.; Vanzo, J. A. *J. Chem. Soc., Chem. Commun.* **1976**, 264. (n) Comba, P.; Engelhardt, L. M.; Harrowfield, J. M.; Lawrence, G. A.; Martin, L. L.; Sargeson, A. M.; White, A. H. *J. Chem. Soc., Chem. Commun.* **1985**, 174. (o) Diamantis, A. A.; Manikas, M.; Salam, M. A.; Snow, M. R.; Tiekink, E. R. T. *Aust. J. Chem.* **1988**, *41*, 453.

(9) (a) *Comprehensive Coordination Chemistry*; Wilkinson, G.; Gillard, R. D.; McCleverty, J. A., Eds.; Pergamon Press: Oxford, England, 1987; Vol. 3, p 453. (b) *Encyclopedia of Inorganic Chemistry*; King, R. B., Ed.; John Wiley & Sons: New York, 1994; Vol. 8, p 4296. (c) *Advanced Inorganic Chemistry*, 5th ed.; Cotton, F. A., Wilkinson, G., Eds.; John Wiley & Sons: New York, 1988; p 665.

(10) Butler, A.; Walker, J. V. *Chem. Rev.* **1993**, *93*, 1937.

(11) Smith, M. J.; Kim, D.; Horenstein, B.; Nakanishi, K.; Kustin, K. *Acc. Chem. Res.* **1991**, *24*, 117.

(12) (a) Shechter, Y.; Karlish, S. J. D. *Nature* **1980**, *284*, 556. (b) McNeill, J. H.; Yuen, V. G.; Hoveyda, H. R.; Orvig, C. *J. Med. Chem.* **1992**, *35*, 1489.

(13) Harris, W. R.; Carrano, C. J. *J. Inorg. Biochem.* **1984**, *22*, 201.

Scheme 1

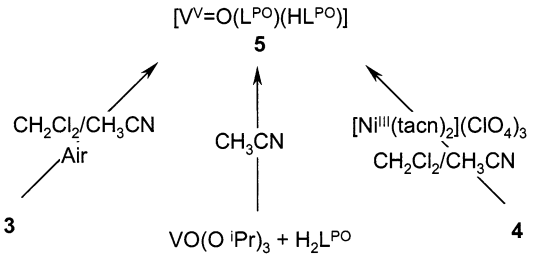

Results and Discussion

The general method for the synthesis of complexes **1**−**4** involves an anaerobic reaction of $[V^{III}(THF)_3Cl_3]$ with the ligands H_2L^X and Et_3N as a base in dry acetonitrile. A short exposure to air of the resulting solution ensures the conversion of V^{III} to V^{IV}, and subsequent storage of the solution under an argon stream to avoid further oxidation and to concentrate the solution yields the desired product. The reactions are clean, affording large quantities of pure crystalline products in good yield (50−80%).

$$2H_2L^X + V(THF)_3Cl_3 + 4Et_3N \xrightarrow[\text{(ii) air}]{\text{(i) } CH_3CN,\ Ar} V^{IV}L^X{}_2 + 4Et_3NH^+ + 3Cl^- + 1e^- + 3THF$$

[X = S (**1**), Se (**2**), P (**3**), PO (**4**)]

Non-oxo V^{IV} complexes **1** and **2** can also be prepared by displacing the oxo group from $VO(acac)_3$ or $VO(H_2O)_5^{2+}$ in CH_3CN with Et_3N as a base under argon. Such displacement of the vanadyl oxygen is known in the literature.[8a,h] These reactions are facilitated by the use of the ligand in its protonated form and the addition of a mild base such as Et_3N. The oxo group may be protonated and released as water.

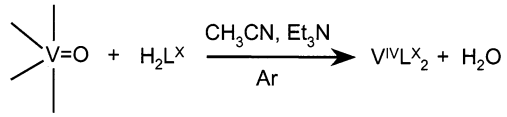

[X = S (**1**), Se (**2**)]

It is noteworthy that this route does not afford the desired products with the ligands H_2L^P and H_2L^{PO}, presumably because of the high basicity of the phenolate oxygens in these ligands. The use of oxovanadium(IV) as a starting material in the syntheses of nonoxovanadium(IV) complexes depends not only on the proper choice of reaction conditions but also on the ability of the chosen ligand to donate sufficient electron density (σ and π) to the metal to stabilize the nonoxo bare species.

Complexes **1**−**4** are stable both in the solid state and in solution under argon. The solutions of **1**−**4** become oxidized rather easily by air. For example, a solution of **3** in CH_2Cl_2/CH_3CN after exposure to aerial oxygen affords **5**, a $V^V = 0$ monomer, in which the ligand L^P of **3** is oxidized to L^{PO}. Complex **5** can also be obtained by direct routes, which are depicted in Scheme 1.

However, the reactions of vanadyl tris-isopropoxide, $VO(O^iPr)_3$, with ligand H_2L^{Se} or H_2L^S yield dinuclear complexes $[V^V{}_2O_2L^X{}_2(\mu_2\text{-}OH)_2]$, **6** and **7**, respectively. The bridging hydroxide ligands are presumably derived from residual water in the solvent.

$$VO(O\,^iPr)_3 + H_2L^X (X = S, Se) \xrightarrow[\text{room temp}]{CH_3CN} [V^V{}_2O_2L^X{}_2(\mu_2\text{-}OH)_2]$$
6, X = Se
7, X = S

Because complex **7**, the sulfur analogue of **6**, has recently been reported in the literature,[14] we will not describe complex **7** again. We will discuss only complex **6** here. It is interesting that **5** is the main isolated product under the condition that favors the dimer formation for the S- and Se-containing ligands.

Selected IR data for complexes **1**−**6** are given in the Experimental Section. The sharp ν(OH) band for the free ligands in the region 3400−3200 cm^{-1} is replaced by a broad band in the complexes indicating that the phenol character of the ligand is lost. There are several strong bands in the region 3000−2800 cm^{-1} due to the ν(C−H) stretchings of the *tert*-butyl or methyl groups. The most important difference between the IR spectra of biscomplexes **1**−**4** and that of **5** and **6**, the vanadyl(V) complexes, is the presence of a strong ν(V═O) stretch at ∼950 cm^{-1} in **5** and **6**. The ν(V═O) frequency is at the lower end of the range 935−1035 cm^{-1} reported for a large number of oxovanadium complexes.[15] Complexes **4** and **5** show strong ν(P═O) stretchings at 1118 and 1121 cm^{-1}, respectively.

Electron ionization (EI) and electrospray ionization (ESI) mass spectroscopy were found to be very important analytical techniques for the characterization of complexes **1**−**5**. The EI mass spectrum (MS) of **1** shows the molecular ion peak at *m*/*z* 931 with an abundance of 100% with the expected isotope pattern. Similarly, complexes **2**, **3**, and **4** show the molecular ion peak at *m*/*z* 1027, 1083, and 1115 (all with 100% abundance), respectively, with an isotopic distribution calculated for those complexes. As a representative example, Figure 1 shows the comparison of the experimental and theoretical isotope pattern of the M^+ ion for **2**. This isotope pattern reflects the natural abundance of metal and ligand atom isotopes.

The EI mass spectrum of **5** shows a molecular ion peak at *m*/*z* 1133 with an abundance of 56%. The peak at *m*/*z* 534 with 100% abundance (base peak) corresponding to ligand H_2L^{PO} is observed as a result of fragmentation. The EI-MS or ESI-MS for **6** does not provide much useful information. In the EI-MS, the peak at *m*/*z* 1027 for **6** corresponds to $VL^{Se}{}_2$, **2** produced in the gas phase. This is an indication of the removal of the oxo group from V═O even at a higher oxidation state in the gas phase.

Complexes **5** and **6** show well-resolved ^{51}V NMR spectra as expected for diamagnetic V^V complexes. In CD_2Cl_2 solution (∼1 mM) at ambient temperature, at least two

(14) Cornman, C. R.; Geiser-Bush, K. M.; Kampf, J. W. *Inorg. Chem.* **1999**, *38*, 4303.

(15) (a) Selbin, J. *Chem. Rev.* **1965**, *65*, 153. (b) Selbin, J. *Coord. Chem. Rev.* **1966**, *1*, 293.

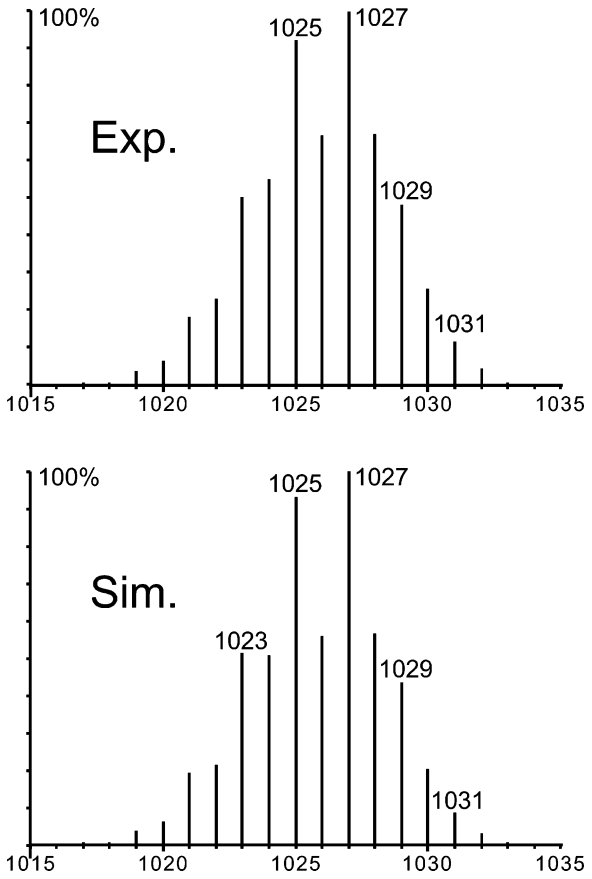

Figure 1. Molecular ion peak in the EI mass spectrum for complex **2** with experimental (Exp.) and calculated (Sim.) isotopic distributions.

species are present for each complex. Complex **5** shows two ^{51}V NMR resonances with a major peak at −430.31 ppm and a peak at −479.92 ppm having significantly higher line width. This increased line width may be because of a combination of quadrupolar broadening and chemical exchange effects. The phenolate and phosphoryl equatorial donors of **6** should impose a greater electric field gradient at the vanadium centers.

Complex **6** shows four resonances at −387.93, −393.34, −400.56, and −404.55 ppm. These four resonances are more likely due to syn/anti and ligand exchange isomers. The addition of excess C_2H_5OH to a CH_2Cl_2 solution of **6** yields a complex with an ethoxide bridge, indicating that the hydroxide bridging ligands are labile. ^{51}V NMR, thus, is a very useful tool to use in characterizing the V^V complexes and to study their isomerization behavior in solution.

Single-Crystal X-ray Diffraction Studies. Complexes **1**−**3** are isostructural with a *fac*-XO_2 donor set (X = hetero donor atom); hence, details of them are not discussed here. Only complex **2** as a representative case is discussed here. Selected bond angles and bond lengths for **1**−**3** are given together in Table 1 for comparison purposes.

Molecular Structure of 2. Single crystals of **2** were isolated from a CH_3CN solution and analyzed by the single-crystal X-ray diffraction method. The analysis confirms that a vanadium complex with M−L = 1:2 is formed. The resulting unit cell contains two independent molecules with similar bond distances and angles. Figure 2 shows the ORTEP diagram of VL^{Se}_2 with the atom-labeling scheme. The complex consists of a neutral unit composed of a central pseudo-octahedral vanadium ion V(1) surrounded by two tridentate ligands bound in a facial manner (*fac*-OSeO donor set). All of the phenols are deprotonated, indicating the +4 oxidation state of the hexacoordinated V(1) center. Two oxygen and two selenium atoms (from two ligand sets) form the best equatorial plane with the deviation $\Delta = 0.0802$ Å, in which two identical donor atoms occupy cis positions with respect to each other. The remaining phenolate oxygen atoms, O(2) and O(2)*, mutually trans, complete the coodination sphere. The phenyl rings are planar, indicating the retention of aromaticity of the rings.

The mean value of the four V−O bond distances of 1.8535(10) Å in VL^{Se}_2 is consistent with the V^{IV} oxidation state, although significantly shorter than that in the catecholate vanadium(IV) complex $[Et_3NH]_2[V^{IV}(cat)_3]\cdot CH_3CN$ (av 1.930(3) Å) [8a] and somewhat longer than that in the $[V^{IV}L][BPh_4]$ complex (L = 1,4,7-tris (5-*tert*-butyl-2-hydroxybenzyl)-1,4,7-triazacyclononane) (av 1.827(5) Å).[8b]

Molecular Structure of 4·3.25CH$_3$CN. Single crystals of *fac*-cis(O,O)-$[VL^{PO}_2]$ were obtained from a CH_3CN solution by slow evaporation of the solvent. The ORTEP diagram for the structure of compound **4** is displayed in Figure 3, whereas selected bond lengths and angles are summarized in Table 2. No substantial differences in bond lengths and angles are found between the two crystallographically independent molecules.

The complex consists of a neutral unit composed of a distorted octahedral vanadium ion surrounded by two ligands with an O, O, P═O donor set in a facial manner. The basic structural difference between complex **4** and other complexes **1**−**3** is the bonding mode of the ligand. Although the ligands are facially coordinated, the axial direction consists of two different types of oxygen donors. This makes the system more distorted along the equatorial plane. Two phenolate oxygens, O(41) and O(9), from two ligands and two phosphoryl oxygens, O(47) and O(7), constitute the equatorial plane, whereas the remaining phenolate oxygen from one ligand and a phosphoryl oxygen from another ligand are trans to each other. Different V−O bond distances, V(1)−O(7) (2.0092(14)Å) and V(1)−O(41) (1.8585(14)Å), make the system distorted, resulting in a O(41)−V(1)−O(7) angle of 170.80(6)°. The V(1)−O(7) (phosphoryl) bond distance is longer than the other V−O(phenolate) bond distances, which might be consequences of both Jahn−Teller distortion, expected for d^1 systems, and of the weak ligand field strength of the phosphoryl oxygens. All of the phenols are deprotonated, and aromatic rings are planar, confirming the formal oxidation state of the central vanadium ion to be +4, which was further established by EPR and magnetic measurements. The P(7)−O(7) and P(47)−O(47) bond lengths, 1.528 and 1.530 Å, respectively, are slightly longer than, as expected, that in free H_2L^{PO}, 1.514 Å.[1d]

Molecular Structure of 5·CH$_3$CN·CH$_2$Cl$_2$. The structure of the complex is shown in Figure 4. Important bond distances and angles are given in Table 3.

Table 1. Selected Bond Lengths (Å) and Angles (deg) for Complexes **1**−**3**

	1 (X = S)	**2** (X = Se)	**3** (X = P)		**1** (X = S)	**2** (X = Se)	**3** (X = P)
		bond lengths				bond angles	
V(1)−O(1)#1	1.8487(10)	1.846(3)	1.909(10)	O(1)#1−V(1)−O(1)	93.23(6)	93.5(2)	102.88(43)
V(1)−O(1)	1.8488(10)	1.846(3)	1.904(10)	O(1)#1−V(1)−O(2)#1	100.34(5)	100.19(14)	103.48(43)
V(1)−O(2)#1	1.8583(10)	1.859(3)	1.872(10)	O(1)−V(1)−O(2)#1	96.28(4)	96.22(14)	91.17(43)
V(1)−O(2)	1.8584(10)	1.859(3)	1.921(10)	O(1)#1−V(1)−O(2)	96.29(4)	96.22(14)	89.44(43)
V(1)−X(1)	2.5306(4)	2.6373(9)	2.476(5)	O(1)−V(1)−O(2)	100.34(5)	100.19(14)	98.47(42)
V(1)−X(1)#1	2.5306(4)	2.6374(9)	2.475(5)	O(2)#1−V(1)−O(2)	155.72(6)	156.0(2)	161.52(43)
				O(1)#1−V(1)-X(1)	82.42(3)	83.29(10)	79.83(33)
				O(2)#1−V(1)-X(1)	85.14(3)	84.72(10)	76.60(33)
				O(2)−V(1)−X(1)	79.68(3)	79.92(10)	75.76(32)
				O(1)#1−V(1−-X(1)#1	82.42(3)	83.29(10)	80.20(32)
				O(1)−V(1)−(1)#1	173.38(3)	174.46(10)	165.51(34)
				O(2)#1−V(1)−X(1)#1	79.69(3)	79.92(10)	90.52(33)
				O(2)−V(1)−X(1)#1	85.15(3)	84.72(10)	75.76(32)
				X(1)−V(1)−X(1)#1	102.34(3)	100.21(5)	101.19(18)

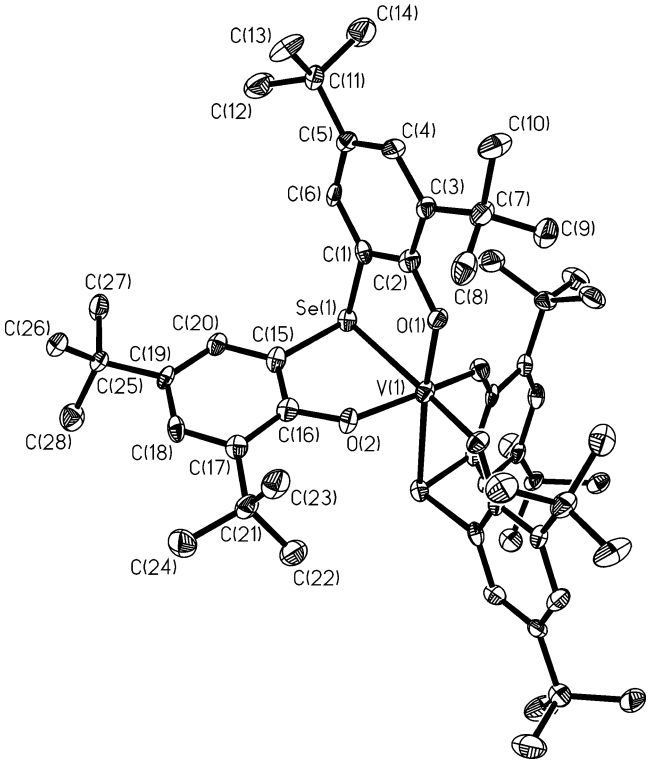

Figure 2. Molecular structure of VL^{Se}_2, **2**.

Complex **5** is mononuclear and can be described as a distorted octahedron with two ligands per oxovanadium(V) unit. One $[L^{PO}]^{2-}$ is coordinated facially through an O, O, O donor set. The second ligand occupies the remaining two equatorial sites using a phenolate oxygen O(3) and the phosphoryl oxygen O(20). The phosphoryl oxygens O(20) and O(10) are cis to each other and bound to V(1) with distinctly different bond distances, V(1)−O(20) = 2.054(2) and V(1)−O(10) = 2.190(2) Å. O(20) is hydrogen bonded to the noncoordinated phenol oxygen, O(4). Phosphoryl oxygen O(10) is bonded trans to vanadyl oxygen O(30), making the axial plane have a O(10)−V(1)−O(30) angle of 176.33(8)°. The V−O(phenolate) bond distances for the facially coordinated ligand are V(1)−O(1) = 1.864(2)Å and V(1)−O(2) = 1.859(2)Å, whereas the similar V(1)−O(3) distance for the other ligand is longer at 1.895(2)Å. The V−O distances are within the range of normal V−O(phenolate) distances. The V(1)−O(30) bond distance (1.604(2)Å) clearly

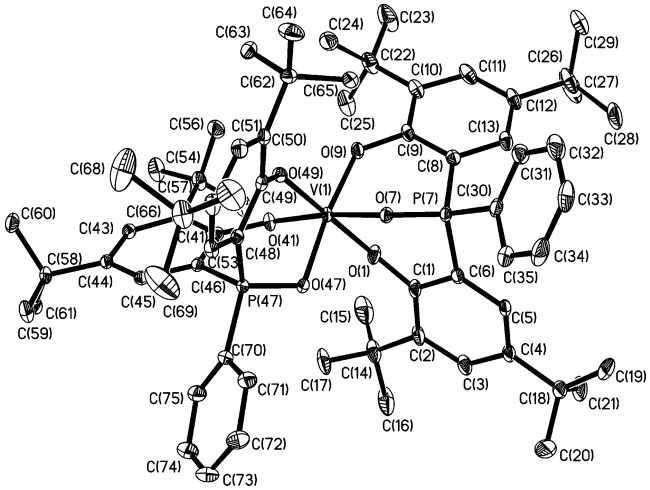

Figure 3. ORTEP representation of VL^{PO}_2, **4**.

Table 2. Selected Bond Distances (Å) and Angles (deg) for Complex **4**·3.25CH_3CN

bond distances		bond angles	
V(1)−O(41)	1.8585(14)	O(41)−V(1)−O(9)	100.76(6)
V(1)−O(9)	1.8785(14)	O(41)−V(1)−O(49)	88.59(6)
V(1)−O(49)	1.8940(14)	O(9)−V(1)−O(49)	91.78(6)
V(1)−O(1)	1.9020(15)	O(41)−V(1)−O(1)	94.52(6)
V(1)−O(47)	2.0090(14)	O(9)−V(1)−O(1)	89.94(7)
V(1)−O(7)	2.0092(14)	O(49)−V(1)−O(1)	176.11(7)
C(6)−P(7)	1.785(2)	O(41)−V(1)−O(47)	88.14(6)
O(7)−P(7)	1.5275(14)	O(9)−V(1)−O(47)	171.10(6)
P(7)−C(8)	1.783(2)	O(49)−V(1)−O(47)	88.77(6)
P(7)−C(30)	1.799(2)	O(1)−V(1)−O(47)	89.00(6)
O(9)−C(9)	1.339(2)	O(41)−V(1)−O(7)	170.80(6)
O(1)−C(1)	1.337(3)	O(9)−V(1)−O(7)	88.03(6)
O(41)−C(41)	1.346(2)	O(49)−V(1)−O(7)	88.42(6)
C(46)−P(47)	1.787(2)	O(1)−V(1)−O(7)	88.15(6)
P(47)−O(47)	1.5300(14)	O(47)−V(1)−O(7)	83.10(6)
P(47)−C(48)	1.787(2)		
P(47)−C(70)	1.801(2)		
O(49)−C(49)	1.342(2)		

indicates the V═O character, and the system is a genuine V^V system, as is also evident from the electroneutral molecular formula with one protonated ligand and its diamagnetism. The benzene rings are planar and retain their aromatic character.

Molecular Structure of 6. The molecular geometry and atom-labeling scheme of dioxodivanadium(V) complex **6** are shown in Figure 5. The structure of the complex consists of a discrete dinuclear centrosymmetric unit having crystal-

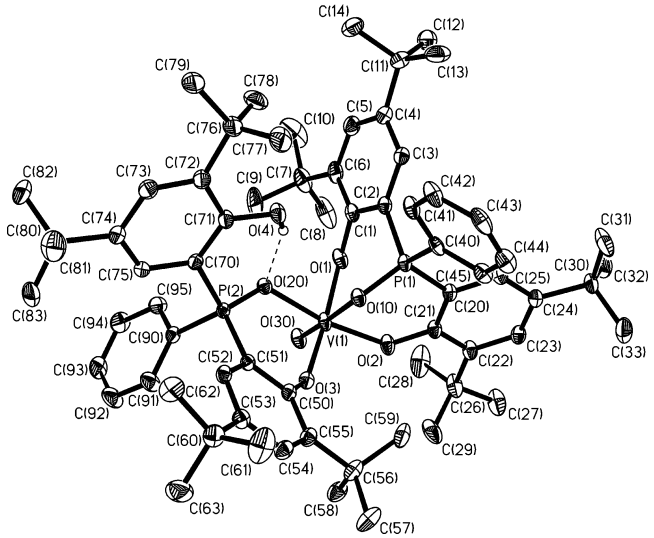

Figure 4. Perspective view of the neutral complex $[VO(L^{PO})(HL^{PO})]$, **5**. Hydrogen bonding involving the hydrogen of the monoprotonated ligand is also shown.

Table 3. Selected Bond Lengths (Å) and Angles (deg) for Complex **5**·CH_2Cl_2·CH_3CN

bond lengths		bond angles	
V(1)−O(30)	1.604(2)	O(30)−V(1)−O(2)	97.80(8)
V(1)−O(2)	1.859(2)	O(30)−V(1)−O(1)	96.05(9)
V(1)−O(1)	1.864(2)	O(30)−V(1)−O(10)	176.33(8)
V(1)−O(10)	2.190(2)	O(30)−V(1)−O(3)	95.10(9)
V(1)−O(3)	1.895(2)	O(30)−V(1)−O(20)	98.28(8)
V(1)−O(20)	2.054(2)	O(2)−V(1)−O(1)	92.02(9)
P(1)−O(10)	1.512(2)	O(2)−V(1)−O(10)	85.52(7)
P(1)−C(20)	1.789(2)	O(2)−V(1)−O(3)	94.26(8)
P(1)−C(40)	1.795(2)	O(2)−V(1)−O(20)	163.69(7)
P(1)−C(2)	1.795(2)	O(1)−V(1)−O(10)	85.37(7)
P(2)−O(20)	1.520(2)	O(1)−V(1)−O(3)	166.35(7)
P(2)−C(51)	1.777(2)	O(1)−V(1)−O(20)	83.65(7)
P(2)−C(90)	1.792(2)	O(10)−V(1)−O(3)	83.05(7)
P(2)−C(70)	1.794(2)	O(10)−V(1)−O(20)	78.48(6)
O(1)−C(1)	1.346(3)	O(3)−V(1)−O(20)	86.97(7)
O(2)−C(21)	1.344(3)		
O(3)−C(50)	1.333(3)		
O(4)−C(71)	1.356(3)		

lographic 2-fold symmetry. Selected bond parameters are listed in Table 4.

This complex is composed of two edge-shared octahedra in which the ligand $[L^{Se}]^{2-}$ coordinates facially with the selenium atom trans to the oxo donor atom. The vanadium atoms are bridged by two hydroxide ligands. Two bridging hydroxide oxygens and two phenolates from the ligand form the equatorial plane. The Se(1)−V(1)−O(4) angle of 174.64(12)° forms the axial plane of the vanadyl-centered distorted octahedron. The hydroxide bridge is symmetric with V(1)−O(3) and V(1)−O(3)# distances of 1.964(3) and 1.969(3)Å, respectively. The axial V(1)−Se(1) and V(1)−O(4) distances are 2.8857(9) and 1.585(3)Å, respectively, clearly indicating the latter as a V═O unit and the oxidation state of the metal center as +5, which is in accord with the ^{51}V NMR spectroscopy.

Electronic Spectroscopy and Magnetic Circular Dichroism Measurements. Electronic spectra for complexes **1**−**6** were measured over the range 200−1200 nm in CH_2Cl_2 solution. In the analyzed region, intra-ligand transitions at higher energies and charge-transfer (CT) transitions at

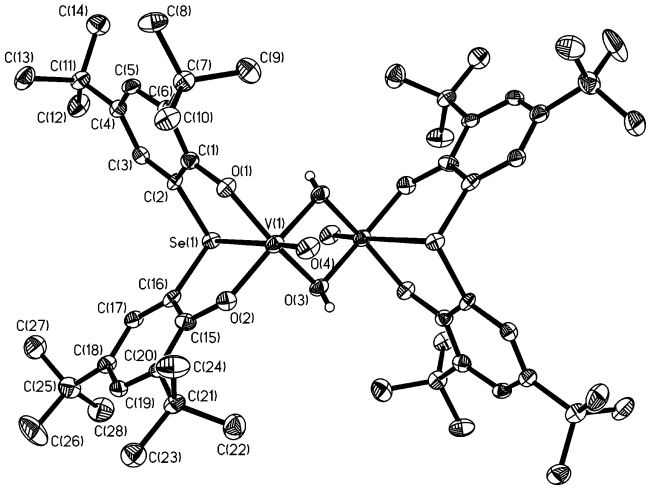

Figure 5. Structure of the violet crystals of $[(VO)_2(L^{Se})_2(\mu\text{-}OH)_2]$, **6**.

Table 4. Selected Bond Lengths (Å) and Angles (deg) for Complex **6**

bond lengths		bond angles	
V(1)−O(4)	1.585(3)	O(4)−V(1)−O(3)	101.3(2)
V(1)−O(3)#	1.969(3)	O(4)−V(1)−O(3)#	100.4(2)
V(1)−O(2)	1.842(3)	O(4)−V(1)−O(1)	100.90(14)
V(1)−V(1)#	3.141(3)	O(4)−V(1)−O(2)	98.3(2)
V(1)−O(3)	1.964(3)	O(4)−V(1)−Se(1)	174.64(12)
V(1)−O(1)	1.850(3)	O(3)−V(1)−O(3)#	74.0(2)
V(1)−Se(1)	2.8857(9)	O(3)−V(1)−O(1)	154.4(2)
		O(3)−V(1)−O(2)	91.74(3)
		O(3)−V(1)−Se(1)	81.96(10)
		O(3)#−V(1)−O(1)	89.68(14)
		O(3)#−V(1)−O(2)	158.32(14)
		O(3)#−V(1)−Se(1)	84.53(10)
		O(1)−V(1)−O(2)	97.37(13)
		O(1)−V(1)−Se(1)	76.95(9)
		O(2)−V(1)−Se(1)	77.21(9)
		V(1)−O(3)−V(1)#	106.0(2)

intermediate energies are expected to be found. In the present case, it appears that the long tail of CT bands obscures low-energy ligand field transitions.

The electronic spectra of complexes **1**−**4** in CH_2Cl_2 solution at room temperature primarily consist of two transitions, a band around 550 nm (18 000 cm^{-1}) and the second band around 400 nm (25 000 cm^{-1}). The lowest-energy bands around 550 nm (18 000 cm^{-1}) are assigned to phenolate-to-vanadium(IV) CT transitions by analogy to other reported bare′ vanadium(IV) complexes[8a−o]. The higher-energy transitions at around 400 nm (25000 cm^{-1}), which are absent in the free ligands, are also assigned to the phenolate-to-vanadium(IV) CT transition. There is also a shoulder at ∼700 nm (14000 cm^{-1}) for complexes **1**−**4**.

To corroborate these assignments, we carried out magnetic circular dichroism (MCD) experiments at liquid helium temperatures on complex **4**. The conclusions are likely to carry over to the other complexes as well given the spectral similarities. Figure 6 shows absorption (ABS) spectra of **4** obtained in butyronitrile solution and low-temperature (5 K) MCD data obtained from a butyronitrile glass. The simultaneous Gaussian resolution of the data reveals the presence of at least six intense electronic transitions between 9000 and 30 000 cm^{-1} (fit parameters are collected in Table 5). Absorption measurements were extended down to 5000 cm^{-1}, and no further transitions were detected. The temper-

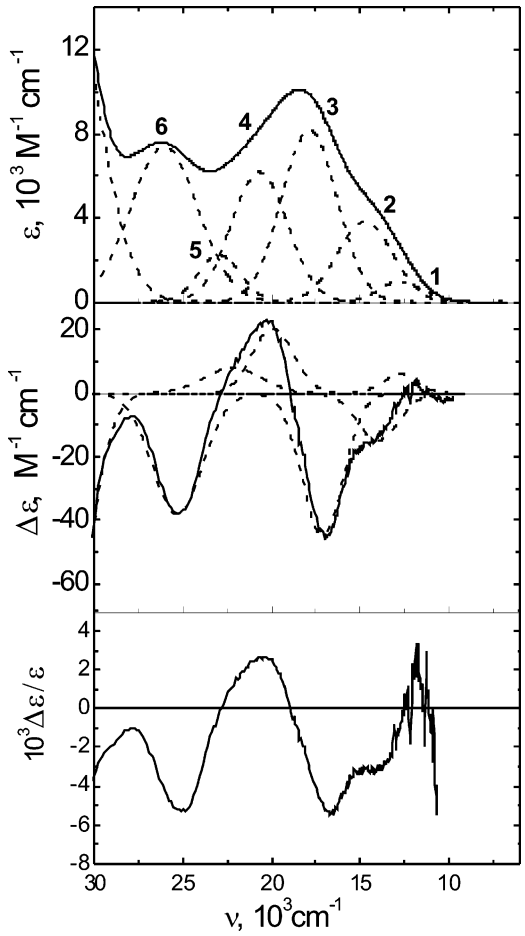

Figure 6. Room-temperature electronic and MCD spectra of **4** in butyronitrile. The MCD spectrum was measured at 5 K.

Table 5. Gaussian Fit Parameters for the Simultaneous Gaussian Resolution of Room Temperature ABS and Low-temperature MCD Spectra[a]

transitions	1	2	3	4	5	6
ν_{max}, 10^3 cm^{-1}	12.7	14.7	17.9	20.7	22.9	26.1
fwhm, 10^3 cm^{-1}	2.89	3.64	3.66	3.69	2.80	4.47
f_{osc}	0.013	0.064	0.138	0.105	0.029	0.152
λ_{max}, 10^3 cm^{-1}	12.8	14.0	17.1	19.9	22.2	25.3
fwhm, 10^3 cm^{-1}	2.25	2.72	2.71	2.73	3.79	3.31
10^3 |C/D|	5.2	3.1	4.2	2.6	4.8	4.0

[a] Slight shifts of up to 700 cm^{-1} in band positions and widths were allowed in the fit.

ature variation of the MCD signal (not shown) shows that all intensity arises from the C-term mechanism, which is expected to dominate the MCD spectra of paramagnetic substances at low temperatures. Saturation magnetization data (also not shown) confirm the $S = {}^1/_2$ state of **4**, which is consistent with EPR and magnetic susceptibility measurements. A useful measure of the character of these transitions is the oscillator strength obtained from absorption spectroscopy as well as C/D ratios, which reflect the relative intensities of the MCD and absorption features for a given electronic transition. Thus, high oscillator strength ($>10^{-4}$) with small C/D ratios (<0.01) reflect CT transitions, whereas low oscillator strengths ($<10^{-4}$) and high C/D ratios of (>0.01) are typically observed for d−d transitions.[22] On the basis of these measures, all electronic transitions observed for **4** should be assigned to CT transitions, most plausibly from the various phenolate ligands. This is also in accord with preliminary resonance Raman measurements on **4**, which showed that laser excitation with 514.5-nm excitation leads to enhancements of vibrational features typically observed for coordinating phenolate moieties. A more detailed assignment of the electronic spectra of **4** based on experimental data alone is a complex task given the presence of four phenolate donors and five possible acceptor orbitals on the central metal and is outside the scope of this paper.

The purple color of complexes **5** and **6** along with their high ϵ value is presumably due to phenolate-to-vanadium CT, as is seen for other oxovanadium(V) complexes of phenolate-derived ligands. The absence of the low-energy transitions, (i.e., >800 nm) suggests that this transition may be due to the trans-$Ar_2Se \rightarrow VO$ chromophore.

Magnetic Susceptibility Studies. Magnetic susceptibility data for polycrystalline samples of complexes **1**−**4** were collected in the temperature range 2−290 K in an applied magnetic field of 1 T. Above 10 K, the temperature-independent magnetic moments of solids **1**, **2**, **3**, and **4** are 1.73 (± 0.03), 1.72 (±0.03), 1.72 (±0.03), and 1.70 (±0.04) μ_B, respectively. These results are consistent with the formulation of the complexes as vanadium(IV) d^1 species (spin-only $\mu_{eff} = 1.73\mu_B$) with insignificant intermolecular coupling and are in complete agreement with the X-ray and EPR results. Simulations of the experimental magnetic moment data yield $g = 1.96$, TIP $= 90 \times 10^{-6}$ emu for **1**, $g = 1.95$, TIP $= 90 \times 10^{-6}$ emu for **2**, $g = 1.97$, TIP $= 40 \times 10^{-6}$ emu for **3**, and $g = 1.94$ for **4**; complexes **5** and **6** are diamagnetic as expected for vanadium(V) with d^0 electronic configuration.

EPR Spectra. EPR spectra of complexes **1**−**4** were measured at the X-band frequency at low temperature in a variety of solvents or solvent mixtures. The EPR spectra of the complexes display the typical eight-line pattern of vanadium (^{51}V; $I = {}^7/_2$).

For systems having a d^1 electronic configuration, covalent bonding becomes progressively more important as the charge on the ion increases. The resultant transfer of charge to the ligands lowers the effective value of the spin−orbit coupling parameter and in some cases may reverse the expected relative magnitudes of g components. According to ligand field (LF) theory, $g_z > g_x = g_y$, the correct ordering of g factors is obtained when the ligands are considered explicitly in the molecular orbital (MO) calculation.[16] For octahedral molecules, the calculations indicate that g_z is affected only by bonding in the equatorial plane, whereas axial bonding on the Z axis affects g_x and g_y.

(16) *Transition Metal Chemistry*; McGarvey, B. R., Carlin, R. L., Eds.; Marcel Dekker: New York, 1966; Vol. 3, p 150.
(17) Jezierski, A.; Raynor, J. B. *J. Chem. Soc., Dalton Trans.* **1981**, 1.
(18) Branca, M.; Micera, G.; Dessi, A.; Sanna, D.; Raymond, K. N. *Inorg. Chem.* **1990**, *29*, 1586.
(19) (a) Kwik, W.-L.; Stiefel, E. I. *Inorg. Chem.* **1973**, *12*, 2337. (b) Stiefel, E. I.; Dori, Z.; Gray, H. B. *J. Am. Chem. Soc.* **1967**, *89*, 3353.
(20) Larsen, S. C. *J. Phys. Chem. A* **2001**, *105*, 8333.
(21) (a) Neese, F. *J. Chem. Phys.* **2001**, *115*, 11080. (b) Neese, F. *Int. J. Quantum Chem.* **2001**, *82*, 104.
(22) Gewirth; A. A.; Solomon, E. I. *J. Am. Chem. Soc.* **1988**, *110*, 3811.

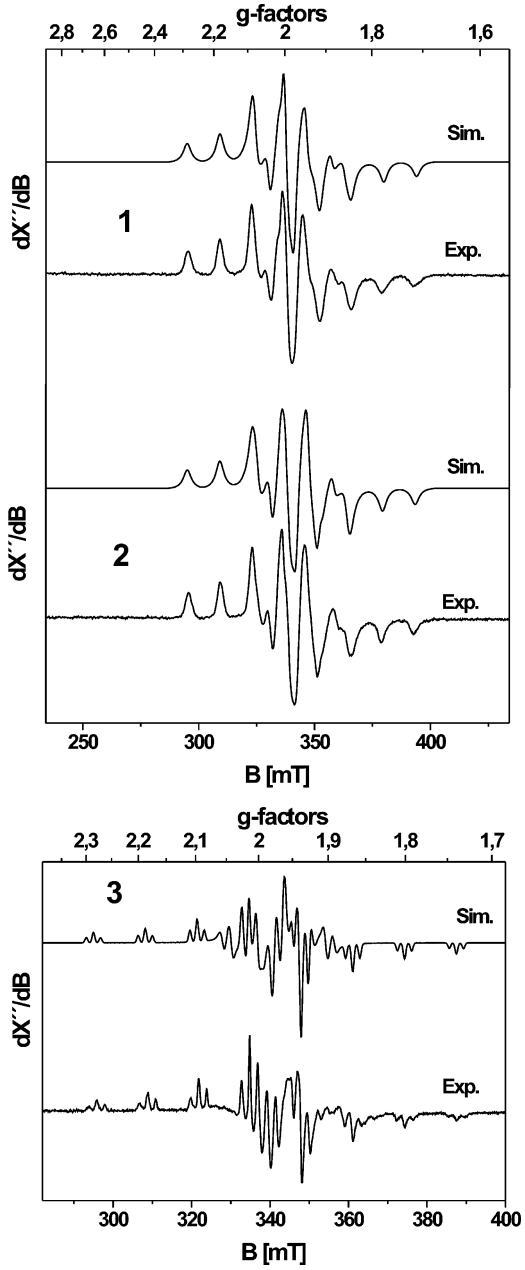

Figure 7. X-band EPR spectra for complexes **1**−**3** in CH_2Cl_2/toluene at 60 K. Experimental conditions: (**1**) microwave frequency 9.44 GHz, microwave power 0.1 mW, modulation amplitude 12.5 G; (**2**) microwave frequency 9.44 GHz, microwave power 0.1 μW, modulation amplitude 12.5 G; (**3**) microwave frequency 9.44 GHz, microwave power 0.1 mW, modulation amplitude 4.96 G. For simulated parameters, see the text.

Six-coordinate vanadium(IV) complexes have been shown[17] from previous EPR studies to fall into two classes, those with a $(d_{xy})^1$ ground-state configuration, which display all $g < 2$ and a large A_z, and those with a $(d_{z^2})^1$ ground state, which display $g_z \approx 2$, g_x, $g_y < 2$ and $A_z \ll A_x$, A_y. The latter parameter can be associated with geometry that is distorted from octahedral toward trigonal prismatic, which requires a relabeling of the axis system such that the three t_{2g} derived orbitals in octahedral symmetry split into an "e" and an "a" (d_{z^2}) set.

The EPR parameters for complexes **1** and **2** clearly place themselves into the category with a $(d_{z^2})^1$ ground-state configuration. This ground state is observed only with complexes having five-membered rings incorporating the central metal ion. Obviously the extra strain in the ring compared with that for six-membered rings must have a dramatic effect upon the electronic structure with consequent reordering of the energy levels. The simulations of the experimental EPR spectra (Figure 7) for **1** and **2** were straightforward and give the parameters $g = \{1.961, 1.957, 1.991\}$, $A = \{49.96, 129.25, 13.08\} \times 10^{-4}$ cm^{-1} for **1** and $g = \{1.956, 1.958, 1.982\}$, $A = \{49.66, 128.45, 19.33\} \times 10^{-4}$ cm^{-1} for **2**. For the sake of simplicity, however, we refrained from exploring the possible rotations of principal axis systems for the g and A matrices. This approximation is not quite justified in view of the results of the electronic structure calculations described below that indicate large noncollinearities between the g and A tensors. Furthermore, the complicated line positions of the hyperfine patterns, which do not follow a completely regular pattern, cannot be simulated without the inclusion of the vanadium nuclear quadrupole interaction. Significant quadrupole effects show up only if the principal axis systems of the quadrupole and hyperfine tensors do not coincide thus further increasing the number of fit parameters. However, the limited resolution of the powder spectra did not allow unique determinations of exact rotation or quadrupole matrices. The problem is even more severe for compounds **3** and **4** (shown below). We note that this situation is a particular feature of the nonoxovanadium(IV) compounds, which in contrast to the oxo complex lack a distinctly short and strong bond that would dominate the ligand field and thereby determine the magnetic coupling tensor orientations (vide infra).

Complexes **1**−**3** form five-membered rings through facially coordinated ligands, where two donor atoms of the same type are trans to each other along the axial direction (from X-ray structure). They are in the same category with other six- coordinate vanadium(IV) complexes with a $(d_{z^2})^1$ ground-state configuration, $[V(mnp)_3]$,[8h] $[V(cat)_3]$,[8a,18] and $[V(mnt)_3]$[19] (mnp = 2-mercapto-4-methylphenolate, cat = catecholate, mnt = maleonitriledithiolate).

Interestingly, the EPR spectrum of complex **3** in a 1:1 solvent mixture of CH_2Cl_2/toluene exhibits superhyperfine coupling from P ($I = {}^1/_2$) for each eight-line pattern due to vanadium. Two phosphorus atoms are directly bonded to the central vanadium, giving rise to five-membered rings and subsequent distortion toward a trigonal prismatic structure. Solvent-dependent hyperfine coupling of phosphorus with vanadium has been observed.[45] To our knowledge, there is

(23) Neese, F. *J. Chem. Phys.* **2001**, *117*, 3939.
(24) Munzarova, M. L.; Kaupp, M. *J. Phys. Chem. A* **1999**, *103*, 9966.
(25) Neese, F. *J. Phys. Chem. A* **2001**, *105*, 4290.
(26) (a) Ballhausen, C. J.; Djurinskij, B. F.; Watson, K. J. *J. Am. Chem. Soc.* **1968**, *90*, 3305. (b) Tachez, M.; Théobald, F. *Acta Crystallogr.* **1980**, *B36*, 249 and 1757. (c) DeMunno, G.; Bazzicalupi, C.; Faus, J.; Lloret, F.; Julve, M. *J. Chem. Soc., Dalton Trans.* **1994**, 1879.
(27) Jørgensen, C. K. *Acta Chem. Scand.* **1957**, *11*, 73.
(28) Ballhausen, C. J.; Gray, H. B. *Inorg. Chem.* **1962**, *1*, 111.
(29) Chaudhuri, P.; Weyhermüller, T. Unpublished results.
(30) Gaffney, B. J.; Silverstone, H. J. In *EMR of Paramagnetic Molecules*; Berliner, L. J., Reuben, J., Eds.; Plenum Press: New York, 1993; Vol. 13.
(31) Neese, F. *Quantum Chemistry Program Exchange Bulletin* **1995**, *15*, 5 (EPR Simulation Program).

no reported EPR study of a vanadium(IV) compound with phosphorus as a donor ligand. The value of g_z decreases compared to that of complexes **1** and **2**. A simulation of the experimental EPR spectrum (Figure 7) for **3** with the approximations discussed above gives the parameters $g = \{1.970, 1.970, 1.975\}$, $A = \{43.3, 43.3, 126.76\} \times 10^{-4}$ cm^{-1}, and $A_{VP} = 21.68 \times 10^{-4}$ cm^{-1}. Because of the limitations mentioned above, these parameters should probably be considered only with care.

In case of complex **4**, different *g* values are obtained. From its structure it is clear that two different types of oxygen are trans to each other forming the axial direction. This leads to a tetragonal distortion along the *z* axis as well as along the *xy* plane. This is seen from the solid-state crystal structure analysis, and the complex shows a higher degree of *g* anisotropy. A reasonable simulation of the particular pattern of hyperfine lines in the X-band spectrum of **4** could not be obtained without including rotations of the hyperfine coupling tensor, *A*, with respect to the principal axes system of the *g* matrix. The low-symmetry condition, which appears to reflect the low molecular symmetry, leads to mixing of different (m_I, m_s) levels and induces unusual EPR transitions in the powder spectrum that are otherwise forbidden. Their contributions, as well as the related shifts of the major transitions, are essential for an acceptable fit of the spectrum of **4**. We applied a genetic algorithm to search the large (nine dimensional) parameter space of principal *g* and *A* values and three Euler angles to find a unique solution of the problem. We found a reasonably good fit, as depicted in Figure 8, with $g = \{1.937, 1.912, 1.844\}$, $A = \{-68, -32, -168\} \times 10^{-4}$ cm^{-1}, and Euler angles $\alpha = -30°$, $\beta = 64°$, and $\gamma = 6°$. Electric quadrupole interaction also might influence the appearance of the EPR spectrum in such a low-symmetry case and might be responsible for the remaining minor misfits. This is almost to be expected for the $3d^1$ configuration of the nonoxovanadium(IV) complexes, which should have a large valence contribution to the electric field gradient tensor, with principal axes that might be different from those of the *A* tensor. Detailed studies of this problem will be the issue of future work based on pulse EPR investigations at X- and Q-band frequencies.

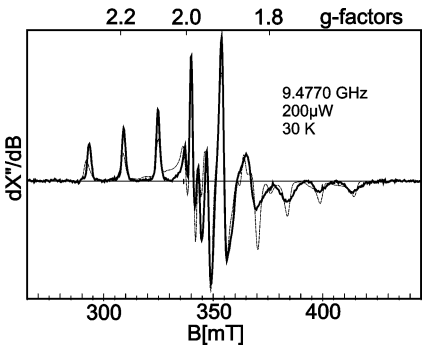

Figure 8. X-band EPR spectrum for complex **4** in butyronitrile/toluene at 30 K. Experimental conditions: microwave frequency 9.477 GHz, microwave power 200 μW, modulation amplitude 5 G. The dashed line is a spin-Hamiltonian simulation as described in the text.

Table 6. Redox Potentials $E_{1/2}$ of Complexes **1**−**6** (in V vs Fc^+/Fc) Obtained from Cyclic Voltammograms in CH_2Cl_2 Solutions

complex	$E_{1/2}$ red	$E_{1/2}$ ox1
1	−0.929	+0.595
2	−0.951	+0.464
3	−1.060	−0.175
4	−0.987	+0.193
5	−0.890	+0.726
6	−0.488	+0.867[a]
	−0.630	

[a] Irreversible, peak potential of oxidation is given.

Complexes **5** and **6** are, as expected, EPR silent, which is consistent with their d^0 electronic configuration.

Electrochemical Results

Cyclic voltammograms (CVs) of complexes **1**−**6** have been measured in CH_2Cl_2 solutions containing 0.1 M Bu_4NPF_6 as the supporting electrolyte at a glassy carbon working electrode and a $Ag/AgNO_3$ reference electrode. Ferrocene (Fc) was used as an internal standard, and the potentials are referenced versus the ferrocenium/ferrocene couple (Fc^+/Fc). From the voltammograms, redox potentials $E_{1/2}$ of the complexes were obtained and are compiled in Table 6.

The cyclic voltammograms of **1**−**5** each display at least two reversible waves, with the exception of dimeric complex **6**, where the oxidation is irreversible. As an example, the cyclic voltammograms of complex **3** at different scan rates are shown in Figure 9. Coulometric experiments show that the waves are due to one-electron-transfer processes. The redox potentials $E_{1/2}$ for the reductions are observed in a narrow range (−0.85 to −1.06 V), irrespective of the nature of the heterodonor, and because phenolato ligands are not reduced in this potential range, we assign these reductions to metal-centered reductions to the V^{III} for complexes **1**−**4** and to V^{IV} for complex **5**.

For complexes **1**−**5**, we performed controlled potential coulometric experiments at appropriate potentials (at −25

(32) Neese, F. *ORCA − An ab Initio, DFT and Semiempirical Electronic Structure Package*, version 2.2, revision 41; Max-Planck Institut für Bioanorganische Chemie: Mülheim, Germany, 2002.
(33) Becke, A. D. *J. Chem. Phys*. **1988**, *84*, 4524.
(34) Perdew, J. P. *Phys. Rev. B* **1986**, *33*, 8822.
(35) (a) Schäfer, A.; Horn, H.; Ahlrichs, R. *J. Chem. Phys*. **1992**, *97*, 2571. (b) Schäfer, A.; Huber, C.; Ahlrichs, R. J. *Chem. Phys.* **1994**, *100*, 5829.
(36) Basis sets were obtained from the ftp server of the quantum chemistry group at the University of Karlsruhe (Germany) at http://www.chemie.uni-karlsruhe.de/PC/TheoChem/.
(37) (a) Pulay, P. *Chem. Phys*. Lett. **1980**, *73*, 393. (b) Pulay, P. *J. Comput. Chem*. **1992**, *3*, 556.
(38) (a) Lee, C.; Yang, W.; Parr, R. G. *Phys. Rev. B: Condens. Matter Mater. Phys.* **1988**, *37*, 785. (b) Becke, A. D. *J. Chem. Phys*. **1993**, *98*, 5648.
(39) Neese, F. *Inorg. Chim. Acta* **2002**, *337C*, 181.
(40) Neese, F.; Solomon, E. I. *Inorg. Chem*. **1998**, *37*, 6568.
(41) Kutzelnigg W.; Fleischer, U.; Schindler, M. In *NMR Basic Principles and Progress*; Diehl, P., Fluck, E., Günther, H., Kosfield, R., Seeling, J., Eds.; Springer: Heidelberg, Germany, 1990; Vol. 23.
(42) (a) Wachters, A. J. H. *J. Chem. Phys*. **1970**, *52*, 1033. (b) Hay, P. J. *J. Chem. Phys.* **1977**, *66*, 4377.
(43) Pastor, S. D.; Spivack, J. D.; Steinhuebel, L. P. *Heterocycl. Chem*. **1984**, *21*, 1285.
(44) (a) Thompson, T.; Pastor, S. D.; Rihs, G. *Inorg. Chem*. **1999**, *38*, 4163. (b) Paine, T. K.; Rentschler, E.; Weyhermüller, T.; Chaudhuri, P. *Eur. J. Inorg. Chem*. **2003**, 3167.
(45) (a) Wasson, J. R. *Inorg. Chem.* **1971**, *10*, 1531. (b) Miller, G. A.; McClung, R. E. D. *Inorg. Chem*. **1973**, *12*, 2552. (c) Lorenz, D. R.; Johnson, D. K.; Stoklosa, H. J.; Wasson, J. R. *J. Inorg. Nucl. Chem.* **1974**, *36*, 1184. (d) Stoklosa, H. J.; Seebach, G. L.; Wasson, J. R. *J. Phys. Chem*. **1974**, *78*, 962.

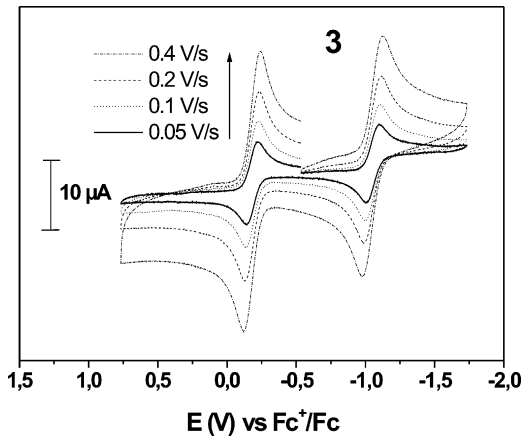

Figure 9. Cyclic voltammogram at ambient temperature of complex **3** in CH_2Cl_2 containing ~1 mM complex and 0.1 M $(n\text{-}Bu)_4NPF_6$ at different scan rates (0.05−0.4 V/s).

°C) in order to generate the reduced and oxidized forms of the complexes and recorded their electronic spectra. In each of the experiments referring to $E_{1/2}^{red}$ and $E_{1/2}^{ox1}$, the current dropped to background levels when one electron per molecule had passed. The stability of the oxidized and reduced forms was confirmed by recording a CV after the electrolysis or by recovery of the starting material's electronic spectra upon voltage reversal. The stabilities were found to be sufficient for the coulometric experiments (30 min at −25 °C) with the exception of the monocation of **5**, which was found to decay in the course of the electrolysis.

In all reductions, it was found that the broad absorption band, which extends from 400 to 700 nm, greatly diminishes during electrolysis and eventually an (almost) colorless solution is obtained. Likewise, the changes in the UV−vis spectra during oxidations exhibit similar features for complexes **1**−**4**; new and very intense absorption grows in two regions, namely around 300−370 nm (for **1**−**4**) and in a second very broad range that extends typically from 500 to 1100 nm. These similarities of the spectral changes provide evidence that the oxidation mechanism is the same for compounds **1**−**4**. Because all monocations were found to be EPR-silent in the temperature range 2−30 K two mechanisms appear feasible, a metal-centered oxidation to a V^V species or the formation of an antiferromagnetically coupled V^{IV}−phenoxyl-radical system. Attempts to prepare monocations by aerial oxidation of **3** or by chemical oxidation of **4** (with $[Ni^{III}(tacn)_2](ClO_4)_3$) for further characterization failed, probably because of the insufficient stability of the oxidized forms. Instead, **5** was obtained in both cases.

However, phenoxyl radicals exhibit a very characteristic electronic spectrum, a band at 400−420 nm and often a single broad band at longer wavelengths with lower intensity. In the present monocations, these features are not met, most of the low wavelength bands are at 300−370 nm, they are spread over a much broader range, and the bands at higher wavelengths are more intense. Therefore, we assign the cations to V^V species.

Molecular Orbital Calculations. To obtain further insight into the electronic structure differences between typical $(VO)^{2+}$ complexes and nonoxo V^{IV}, density functional theory (DFT) as well as INDO/S-CI calculations were carried out on complexes **3** and **4** and, for comparison, on the prototypical complex $[VO(H_2O)_5]^{2+}$, which has already been studied theoretically.[20,23]

The optimized geometry of **4** at the BP86 level is in reasonable agreement with the experimentally determined structure. In particular, the $V-O_{phenolate}$ distances are calculated in good agreement with experiment. However, the distances to the more weakly coordinating P−O groups are calculated to be too long by ~0.1 Å. This is in agreement with our general experience that DFT calculations at the GGA level tend to give rather accurate values for strong metal−ligand bonds although weaker ones are predicted to be significantly too long.

The calculated electronic structure and properties were derived from single-point B3LYP calculations on the optimized structures. The singly occupied MO (SOMO) was obtained from the natural orbitals of the spin-unrestricted Kohn−Sham calculation and is shown in Figure 10. As expected from ligand field theory for a d^1 complex, this orbital is derived from the vanadium t_{2g} set and is reasonably consistent with a "tetragonal ground state" assignment, which differentiates **4** from the other complexes investigated in this study. The SOMO orbital is oriented correctly for π interactions with the coordinating P−O groups in a cis arrangement. Our interpretation of this finding is that the P−O groups are much poorer π donors than the phenolates. Consequently, the lowest-energy MO within the metal t_{2g} set will be the one that has the least π-antibonding interactions with the four phenolate donors. This is also consistent with the calculated Löwdin V−O bond orders that are 0.58 for the V−O−P bonds and 1.01 and 0.98 for the axial and equatorial phenolates, respectively.

In the spin-unrestricted calculations, the four lowest unoccupied spin-up as well as the five lowest unoccupied spin-down MOs are mainly of vanadium character, which is consistent with its formal d^1 electronic configuration. The energetic ordering of these orbitals also follows the pattern expected from LF theory with the three π-antibonding MOs being lower and the two σ-antibonding MOs being higher in energy. The spin contamination of the spin-unrestricted wave function is significant. The vanadium spin density according to a Löwdin analysis amounts to ~1.07 electrons (essentially all of which is found in the metal d shell), which is compensated by slightly negative spin densities on the ligands. The expectation value $\langle S^2 \rangle$ was found to be 0.768.

The calculated EPR parameters (Tables 7, 8, and 9) according to the procedures in ref 21 for the g tensor and ref 23 for the ^{51}V hyperfine coupling (HFC) are in reasonable agreement with the experimental measurements, except, as expected, for the metal hyperfine interaction. As expected from the work of Munzarova and Kaupp[24] and also observed in ref 23, the calculated ^{51}V HFC from B3LYP calculations is in only qualitative agreement with experiment. Quantitative agreement is mainly prevented by the failure of present day DFT methods to describe the core-level spin polarization correctly, which is crucial in order to obtain accurate values

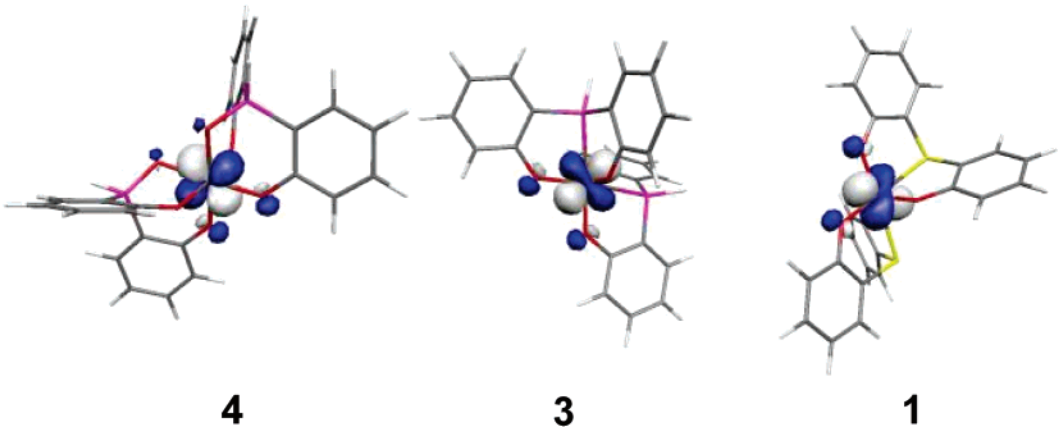

Figure 10. Singly occupied natural orbitals of **4**, **3**, and **1** from spin-unrestricted B3LYP DFT calculations.

for the isotropic Fermi contact term. However, the deviations are fairly systematic and always in the direction of an underestimation of the absolute value of the isotropic HFC value. Scaling of this term with a factor of 1.2−1.3 for V^{IV}-containing systems is probably appropriate and brings the calculated values into much closer agreement with the numbers obtained from the spin-Hamiltonian fitting procedures.

The results of the calculations for **3** are similar to those obtained for **4**. The axial and equatorial $V-O_{phenolate}$ distances are rather well predicted (1.872_{exptl} versus 1.880_{calcd} Å and 1.909_{exptl} versus 1.891_{calcd} Å, respectively). However, the distances to the more weakly coordinating phosphine groups are overestimated by 0.126 Å (2.475_{expd} versus 2.601_{calcd} Å). The calculated Löwdin bond orders are 0.65 for the V−P bonds, thus indicating them to be slightly stronger than the V−O−P bonds in **4**, and 1.04 and 1.01 for the axial and equatorial $V-O_{phenolate}$ bonds, which are comparable to those for **4**. The SOMO of **3** lies in the plane that contains the two P atoms and two phenolate donors. Again, this orbital appears to minimize the π-antibonding interactions with the ligands (Figure 10). In qualitative agreement with the discussion provided in the experimental EPR section, this orbital is consistent with a "trigonal" ground state for this complex as is also reflected in the calculated and observed EPR parameters. The spin densities and $\langle S^2 \rangle$ were virtually identical to those found for **4**.

The calculated EPR parameters for **3** (Table 8) are in acceptable agreement with the experimental values. Similarly to **4**, the calculations predict a somewhat rhombic *g* tensor that could not be resolved in X-band EPR measurements, but the mean value is in good agreement with the experimentally derived values. The calculated ^{51}V HFC is in reasonable agreement with experiment, but the largest value is again too small in magnitude, which is the expected behavior. The calculated ^{31}P HFC is in good agreement with the experimental findings. Perhaps the anisotropy is slightly overestimated, which appears to be typical of DFT calculations.[25] It is interesting that all principal values are negative, which is derived from the negative spin densities at the P atoms. Note that from the spin-Hamiltonian fits only the absolute values of the HFC tensor are available. The ^{51}V HFC and the *g* tensor are very noncollinear. The *g*-tensor axes essentially coincide with the molecular axes. The ^{51}V HFC $+6 \times 10^{-4}$ cm^{-1} component is oriented along the g_{max} direction whereas the other two components bisect g_{min} and g_{mid}. The ^{31}P HFC has significant contributions from the second-order spin−orbit term, which amounts to up to 3×10^{-4} cm^{-1}. It is very noncollinear with the *g* tensor. Finally, we also extended the calculations to complex **1**, which features an O_4S_2 ligand set. The optimized geometry shows the same trend as for the other two examples; namely, the $V-O_{phenolate}$ distances are predicted accurately with errors of less than 0.02 Å whereas the V−S bonds are predicted to be too long by ~0.15 Å. The calculated *g* tensor is rhombic with principal values that are in rather nice agreement with the experimental values from either the B3LYP or INDO/S calculations with a slight advantage for B3LYP (Table 9). The calculated ^{51}V HFC tensor is, again, only in qualitative agreement with experimental values, which is the expected behavior. Note, however, that the calculated HFC tensor is once more very noncollinear with the *g* tensor, which is not taken into account in the EPR simulations, and therefore the correlation with the experimental values is somewhat flawed.

Table 7. Calculated EPR Parameters for **4**[a]

		min	mid	max
g	B3YLP	1.935	1.961	1.973
	INDO/S	1.923	1.936	1.968
	exp	1.844	1.912	1.937
$A(^{51}V)/10^{-4}$ cm^{-1}	B3LYP[b]	−121	−16	−22
	exp[c]	−168	−32	−68

[a] The sign of the HFC is not known from experiment. [b] Euler angles relative to the B3LYP *g* tensor: α, *β*, *γ* = −2°, 36°, and −21°. [c] Euler angles exp(−30, 64, 6°).

Table 8. Calculated EPR Parameters for **3**[a]

		min	mid	max
g	B3LYP	1.954	1.978	1.983
	INDO/S	1.940	1.966	1.977
	exp	1.975	1.970	1.970
$A(^{51}V)/10^{-4}$ cm^{-1} [b]		−105	−34	+6
	exp	−120	31	31
$A(^{31}P)/10^{-4}$ cm^{-1} [c]		−17	−15	−13
	exp	17	20	20

[a] The sign of the HFC is not known from experiment. [b] Euler angles relative to the B3LYP *g* tensor: α, *β*, *γ* = 82°, 2°, and −27°. [c] Euler angles relative to the B3LYP *g* tensor: α, *β*, *γ* = 32°, 140°, and 12°.

Table 9. Calculated EPR Parameters for **1**[a]

		min	mid	max
g	B3LYP	1.977	1.951	1.987
	INDO/S	1.968	1.936	1.984
	exp	1.961	1.957	1.991
$A(^{51}V)/10^{-4}$ cm^{-1} [b]		−106	−35	7
	exp	(−)129	(−)50	13

[a] The sign of the HFC is not known from experiment. [b] Euler angles relative to the B3LYP *g*-tensor: $\alpha, \beta, \gamma = -50°, 0°$, and $-72°$.

Table 10. Calculated EPR Parameters for $[VO(H_2O)_5]^{2+}$

		min	mid	max
g	B3LYP	1.951	1.983	1.983
	INDO/S	1.937	1.986	1.987
	exp	1.933/1.936	1.978/1.982	1.978/1.982
$A(^{51}V)/10^{-4}$ cm^{-1}	B3LYP	−165	−55	−52
	exp	−182	−71	−71

The calculated SOMO (Figure 10) is very similar to that for **3** and nicely shows the trigonal distortion resulting in a $(d_z^2)^1$-type ground state.

Oxo versus Nonoxo V^{IV}. To obtain more insight into the results of the calculations and to shed more light on the differences between oxo and nonoxo V^{IV}, additional calculations were carried out for the typical VO^{2+} complex $[VO(H_2O)_5]^{2+}$. The ligand field in this complex is dominated by an extremely short and strong V≡O triple bond (calculated V≡O distance 1.574 Å versus 1.577−1.591 Å observed experimentally[26]), as has already been pointed out by the pioneers of LF theory.[27,28] Furthermore, a strong trans effect is observed, which leads the axial water to bind at much longer distances (∼2.18 Å) than those of the equatorial waters (∼2.05 Å).

The calculated EPR parameters for $[VO(H_2O)_5]^{2+}$ compare favorably with experimental values. The $g_\perp$ value is accurately predicted from all calculations although the semiempirical INDO/S-CI method appears to be even more successful for the prediction of the $g_{||}$ value than the B3LYP method. The calculated ^{51}V HFCs show the expected behavior because the underestimation of the core-level spin polarization the calculated isotropic value is too positive leading to an underestimation of both $A_{||}$ and $A_\perp$. However, the anisotropy $A_{||} - A_\perp$ is in excellent agreement with experiment, indicating that the main problem indeed comes from the Fermi term.

To interpret the computational results it is instructive to recall the physical origin of the *g* tensor in VO^{2+} systems (Table 10). The striking feature of the VO^{2+} unit is the exceptionally strong π interactions between the central vanadium and the oxo ligand. This splits the t_{2g} orbitals apart by ∼2 eV, which is consistent with accepted spectral assignments.[27,28] Within the nonoxo V^{IV} complexes studied here, the π interactions are much weaker, thus leading to a far less pronounced t_{2g} orbital splitting. From Table 11, the splittings are ∼0.5−1 eV for **3** and **4**. The $g_\perp$ value arises from orbital currents that are induced from excited states in which an electron is promoted from the d_{xy}-based SOMO into the d_{xz}- and d_{yz}-based MOs. The current, and therefore the *g* shift, is larger the more metal character these orbitals have and the smaller the energetic gap between the donor and acceptor orbitals is. Thus, a highly covalent π-interaction in the VO^{2+} core reduces the metal character in the $d_{xz,yz}$ orbitals, which together with the large energetic gap leads to values of $|\Delta g_\perp|$ that are rather small. This is in contrast to the calculations and observations for **3** and **4** that feature higher metal character in the d_π orbitals as well as smaller energetic gaps. Thus, much larger $g_\perp$ shifts are expected. The combination of theory and experiment shows that the $g_\perp$ shifts (deviations from the free-electron *g* value) in **3** and **4** are indeed up to a factor of 3 larger than in $[VO(H_2O)_5]^{2+}$, which nicely correlates with the computed orbital energy differences. The $g_{||}$ shift arises mainly from the excited ligand field state in which an electron is promoted from the d_{xy}-based SOMO into the $d_{x^2-y^2}$-based MO, the energy of which is mainly determined from the σ interactions with the equatorial ligands. This interaction is intrinsically a factor of ∼4 more effective for producing *g* shifts than the excitations in the d_π-orbitals. This is particularly true for VO^{2+}-containing complexes where the energies of the d_π and $d_{x^2-y^2}$ orbitals are comparable. Thus, similar $g_{||}$ shifts are expected for **3**, **4**, and $[VO(H_2O)_5]^{2+}$. For **3**, this expectation appears to be true; the measured *g* tensor is essentially isotropic, and the calculated *g* tensor shows a $g_{||}$ shift close to that of $[VO(H_2O)_5]^{2+}$. The $g_{||}$ of **4** appears to be anomalous and we presently have no satisfactory explanation for its unusual value, but the problem may well be rooted in the complexity of the experimental spectrum. In summary, the calculations show, that the main electronic structural and spectroscopic differences between oxo V^{IV} and nonoxo V^{IV} can be explained by a lack of highly covalent π interactions in the latter case.

Table 11. Comparison of Orbital Energy Differences (in eV) within the Vanadium d-shell for Complexes **3** and **4** vs $[VO(H_2O)_5]^{2+}$ from BP86 DFT Calculations

	Δ_1 $xy \rightarrow xz$	Δ_2 $xy \rightarrow yz$	Δ_3 $xy \rightarrow x_2$-y_2	Δ_4 $xy \rightarrow z_2$
4	0.53	0.58	2.49	2.60
3	0.71	1.28	2.12	2.43
$[VO(H_2O)_5]^{2+}$	1.99	2.08	2.56	4.00

Concluding Remarks

This paper has described ligating properties of four tridentate bisphenol ligands with either [O, S, O], [O, Se, O], [O, P, O], or [O,P═O,O] donor atoms toward the vanadium center. As expected, bis(homoleptic) neutral enigmatic nonoxovanadium(IV) complexes such as $[V^{IV}L_2]$ have been isolated because of the matched charge neutralization of V^{IV} by four phenolate groups, and the compounds have been structurally, both of geometric and electronic nature, thoroughly studied. X-ray structural studies have shown the facial coordination mode of the ligands.

Emphasis has been given in this work to structural and electronic effects arising from the incorporation of a soft heterodonor atom, S, Se, P, or P═O, between the phenolic rings, which can be compared with our earlier work[1j] on nonoxovanadium(IV) with a ligand containing [O, N, O] donor atoms. The realization that the present phenol-

containing ligands can stabilize six-coordinate nonoxovanadium(IV) complexes highlights the prospect of designing a generic ligand system that should generate nonoxovanadium(IV) species with other coordination numbers. Actually, we have already structurally characterized[29] a trigonal bipyramidal nonoxovanadium(IV) with a tripodal phenol-containing ligand.

Electrochemical results suggest that the electrochemical oxidations are not ligand-centered (i.e., no formation of phenoxyl radicals from the coordinated phenolates) but metal-centered generating V^V species. Thus, no stabilization of the V^{IV}−phenoxyl-radical species has been observed.

The investigated molecules in this paper form an interesting series because they allow the properties of V^{IV} to be explored in the absence of a strongly dominating oxo ligand. In particular, from a combination of contemporary DFT and experimental investigation, we found that the ground state of such systems is quite flexible. Thus, **4** with phophoryl donor groups shows a tetragonal ground state whereas **1** and **3** show a trigonal ground state. We suspect that this striking difference is mainly due to the altered ring size in **4** as compared to that in **1** and **3** as well as pronounced differences in the π-bonding ability of a phosphoryl group compared to that of a thioether or a phosphine ligand. Interestingly, our computations fail to reproduce the very large g shift below 1.9 in **4**. This large value indicates that the three t_{2g} orbitals are nearly degenerate, which would lead to very efficient spin−orbit coupling of the three components of the $^2T_{2g}$ ground term and consequently also a large g_{min} shift. Apparently, therefore, the phosphoryl groups are probably even weaker π donors as predicted by the calculations. The absence of a strong V≡O triple bond also leads to pronounced noncollinearities between the g and ^{51}V A tensors (and perhaps also the ^{51}V quadrupole tensor), which greatly complicated the analysis of the experimental EPR spectra. However, this opens an interesting avenue for further investigations using state-of-the-art high-resolution double-resonance techniques. The results of such investigations, which are currently being explored in our laboratory, should be of direct relevance to the study of nonoxovanadium enzymes, which also exist in low-symmetry coordination environments. The theoretical study presented above sheds some light on the electronic structure differences between oxo and nonoxo V^{IV} systems through comparison with the prototype complex $[VO(H_2O)_5]^{2+}$. The results underline the difficulty of predicting quantitatively correct EPR spectroscopic parameters from DFT, in particular for the central metal hyperfine coupling. In this respect, it is noteworthy that the simple INDO/S method has given results that are of similar quality albeit at about 3 orders of magnitude smaller computational cost, which may be significant for the qualitative and semiquantitative exploration of larger systems.

Experimental Section

Materials and Physical Measurements. Commercial-grade chemicals were used for synthetic purposes, and solvents were distilled and dried before use. Fourier transform infrared spectroscopy on KBr pellets was performed on a Perkin-Elmer 2000 FT-IR instrument. Solution electronic spectra were measured on a Perkin-Elmer Lambda 19 spectrophotometer. Mass spectra were recorded either in the EI or ESI (in CH_2Cl_2) mode with a Finnigan MAT 95 or 8200 spectrometer. Magnetic susceptibilities of the polycrystalline samples were recorded on a superconducting quantum interference device magnetometer (MPMS, Quantum Design) in the temperature range 2−290 K with an applied field of 1 T. Diamagnetic contributions were estimated for each compound by using Pascal's constants. Cyclic voltammetry and coulometric experiments were performed using an EG&G potentiostat/galvanostat. X-band EPR spectra were recorded on a Bruker ESP 300E spectrometer equipped with a helium flow cryostat (Oxford Instruments ESR 910), an NMR field probe (Bruker 035M), and a microwave frequency counter HP5352B. Spin-Hamiltonian simulations of the EPR spectra were performed either with a program that was developed from the routines of Gaffney and Silverstone[30] that specifically makes use of the resonance-search procedure based on a Newton−Raphson algorithm as described therein or a previously reported program.[31] A genetic algorithm routine and downhill SIMPLEX techniques were applied to find unique solutions for the simulation parameters. NMR experiments were carried out on a Bruker ARX spectrometer (400 MHz).

Magnetic circular dichroism spectra were obtained on a home-built instrument consisting of a JASCO J-715 spectropolarimeter and an Oxford Instruments SPECTROMAG magnetocryostat, which is capable of generating magnetic fields up to 11 T. Spectra were taken for samples dissolved in butyronitrile which resulted in high-quality glasses suitable for optical spectroscopy at low temperatures. Simultaneous Gaussian resolution of absorption and MCD spectra were performed using Microsoft Excel. C/D ratios were calculated by

$$\frac{C}{D} = \frac{k_B T}{\mu_B B} \frac{\int \frac{\Delta\epsilon(\nu)}{\nu} d\nu}{\int \frac{\epsilon(\nu)}{\nu} d\nu}$$

All DFT calculations reported in this paper were done with the program package ORCA.[32] Unless otherwise indicated, all geometry optimizations were carried out at the BP86 level[33,34] of DFT. This functional has proved in many applications its ability to predict structures of transition-metal complexes reliably. The all-electron Gaussian basis sets used were those reported by the Ahlrichs group.[35] Accurate triple-ζ valence basis sets with one set of polarization functions on the vanadium, oxygen, and phosphorus atoms were used (TZV(P)).[35b] The carbon and hydrogen atoms were described by a slightly smaller split-valence (SV) basis set that is of double-ζ quality in the valence region.[35a] The auxiliary basis sets used to fit the electron density were taken from the TurboMole library[36] and were chosen to match the orbital basis.

Unless otherwise indicated, the self-consistent field calculations were of the spin-polarized type and were tightly converged (10^{-7} Eh in energy, 10^{-6} Eh in density change, and 10^{-6} in maximum element of the DIIS[37] error vector). The geometries were considered to be converged after the energy change was less than 10^{-5} Eh; the gradient norm and maximum gradient element were smaller than 5×10^{-4} Eh/Bohr and 10^{-3} Eh/Bohr, respectively.

Single-point calculations with the B3LYP functional[33,38] were carried out at the optimized geometries in order to predict EPR spectral parameters.[21−23,25,40] In these calculations, the same basis sets were used as in the geometry optimization except for the metal basis, which was the triply polarized "core properties" (CP(PPP)) basis described earlier,[39] and for phosphorus, we used the accurate

Table 12. Crystallographic Data for **1**, **2**, and **3**

	1	**2**	**3**
empirical formula	$C_{56}H_{80}VS_2O_4$	$C_{56}H_{80}VSe_2O_4$	$C_{68}H_{90}P_2VO_4$
formula weight	932.26	1026.06	1084.35
temperature	100(2) K	100(2) K	100(2) K
wavelength (Mo Kα)	0.71073 Å	0.71073 Å	0.71073 Å
crystal system	orthorhombic	orthorhombic	monoclinic
space group	*Pccn* (No. 56)	*Pccn* (No. 56)	*C*2/*c* (No. 15)
unit cell dimensions	$a = 19.6860(12)$ Å, $b = 15.4480(12)$ Å, $c = 18.1887(12)$ Å, $\beta = 90°$	$a = 19.4267(11)$ Å, $b = 15.3404(9)$ Å, $c = 18.8858(11)$ Å, $\beta = 90°$	$a = 20.282(6)$ Å, $b = 18.965(6)$ Å, $c = 36.913(11)$ Å, $\beta = 99.57(4)°$
volume (Å^3), *Z*	5529.2(7), 4	5628.2(6), 4	14001(7), 8
density (calcd) Mg/m^3	1.120	1.211	1.029
absorp coeff/mm^{-1}	0.296	1.510	0.228
data/restraints/param	10340/0/285	4412/0/285	5639/0/296
goodness of fit on F^2	1.024	1.024	1.037
final R indices [$I > 2\sigma(I)$]	R1 = 0.0506, wR2 = 0.1207	R1 = 0.0570, wR2 = 0.1003	R1 = 0.1185 wR2 = 0.2643
R indices (all data)	R1 = 0.0826, wR2 = 0.1483	R1 = 0.1107, wR2 = 0.1155	R1 = 0.2306 wR2 = 0.3202
residual electron density/e Å^{-3}	0.547 and −0.650	0.562 and −0.438	1.154 and −0.370

Table 13. Crystallographic Data for **4**, **5**, and **6**

	4	**5**	**6**
empirical formula	$C_{68}H_{90}VP_2O_6 \cdot 3.25CH_3CN$	$C_{68}H_{91}VP_2O_7 \cdot CH_2Cl_2 \bullet CH_3CN$	$C_{64}H_{94}V_2Se_2O_8N_4$
formula weight	1249.71	1259.27	1307.23
temperature	100(2) K	100(2) K	100(2) K
wavelength (Mo Kα)	0.71073 Å	0.71073 Å	0.71073 Å
crystal system	triclinic	triclinic	monoclinic
space group	$P\bar{1}$ (No. 2)	$P\bar{1}$ (No. 2)	$P2_1/n$ (No. 14)
unit cell dimensions	$a = 17.3782(8)$ Å, $b = 20.5903(8)$ Å, $c = 22.8046(10)$ Å, $\alpha = 75.47(1)°$ $\beta = 70.57(1)°$ $\gamma = 74.30(1)°$	$a = 14.5723(9)$ Å, $b = 15.9764(12)$ Å, $c = 18.0224(14)$ Å, $\alpha = 83.66(2)°$ $\beta = 73.39(2)°$ $\gamma = 65.61(2)°$	$a = 17.625(2)$ Å, $b = 9.6819(9)$ Å, $c = 20.108(2)$ Å, $\beta = 95.31(1)°$
volume (Å^3), *Z*	7290.9(5), 4	3661.8(5), 2	3416.6(6), 2
density (calcd) Mg/m^3	1.139	1.142	1.271
absorp coeff/mm^{-1}	0.230	1.300	1.390
data/restraints/param	33437/32/1645	23670/10/759	5942/0/367
goodness of fit on F^2	1.029	1.084	1.026
final R indices [$I > 2\sigma(I)$]	R1 = 0.0516, wR2 = 0.1149	R1 = 0.0744, wR2 = 0.2341	R1 = 0.0496, wR2 = 0.1120
R indices (all data)	R = 0.0769, wR2 = 0.1271	R = 0.1134, wR2 = 0.2571	R1 = 0.0915, wR2 = 0.1287
resudual electron density/e Å^{-3}	0.574 and −0.492	1.448 and −1.584	0.863 and −0.462

IGLO-III basis.[41] Special care was taken in the numerical integration procedure to integrate accurately the spin density in the core region in the presence of very steep basis functions.[39] In addition, the vanadium basis contained two polarizing p functions with Wachters exponents[42−44] and one additional f function from the TurboMole library with exponent 1.8.[36]

X-ray Crystallographic Data Collection and Refinement of the Structures. Single crystals of **1**−**6** were coated with perfluoropolyether, picked up with glass fibers, and mounted on a Nonius Kappa-CCD diffractometer (**1** and **4**) or Bruker SMART system (**2**, **3**, **5**, and **6**) equipped with a cryogenic nitrogen cold stream operating at 100(2) K. Graphite monochromated Mo Kα radiation ($\lambda = 0.71073$ Å) was used. Intensity data were corrected for Lorentz and polarization effects. The intensity data set of **2**, **5**, and **6** were corrected for absorption with the use of the program SADABS, that for **1**, with MulScanAbs (Pluton 99, Program suite, A. L. Spek, University Utrecht, The Netherlands, 1999), and that for **4**, with the Gaussian face-indexed routine (XPREP, ShelXTL package). The intensity data set of **3** was not corrected. The Siemens SHELXTL software package (G. M. Sheldrick, Universität Göttingen) was used for solution, refinement, and artwork of the structure, and neutral atom scattering factors of the program were used. All structures were solved and refined by direct methods and difference Fourier techniques. Non-hydrogen atoms were refined anisotropically, and hydrogen atoms were placed at calculated positions and refined as riding atoms with isotropic displacement parameters. Details of data collection and structure refinements are summarized in Tables 12 and 13.

Ligand Synthesis. The ligands H_2L^S,[43] H_2L^P,[1d] and H_2L^{PO} [1d] were synthesized according to the published procedures. The ligand H_2L^{Se} was synthesized according to a modification of the method described by Pastor et al.[44]

General Method of Synthesis for V(IV) Complexes 1−4. In a degassed CH_3CN solution (40 mL) of the ligand (1 mmol), $V(THF)_3Cl_3$ (0.5 mmol, 0.186 g) was dissolved. To that violet solution 0.5 mL of Et_3N was added, and the resulting solution was refluxed under argon for 0.5 h. After being cooled to room temperature, the solution was opened to air and stirred for 5 min. The solution was then kept under a slow sweep of argon to yield crystalline solids.

Complex VL^S_2 (1). Yield: 0.38 g (82%). Anal. Calcd for $C_{56}H_{80}S_2O_4V$ (932.31 g/mol): C, 72.15; H, 8.65; S, 6.88; V, 5.46. Found: C, 71.5; H, 8.7; S, 7.6; V, 6.1. IR (cm^{-1}): 3423(br), 2959−2868(s), 1431(s), 1245(s), 1098, 838, 749, 565. Absorption spectrum

(CH_2Cl_2); λ_{max}(nm), ϵ(M^{-1} cm^{-1}): 400(sh), 7190; 531, 7950; 700-(sh), 3430. MS(EI): m/z = 931 [M^+, 100%].

Complex VL^{Se}_2 (2). Yield: 0.46 g (90%). Anal. Calcd for $C_{56}H_{80}Se_2O_4V$ (1026.11 g/mol): C, 65.55; H, 7.86; V, 4.96. Found: C, 65.3; H, 8.0; V, 5.2. IR (cm^{-1}): 3452(br), 2955−2866-(s), 1429(s), 1253(s), 1092, 836, 739, 561. Absorption spectrum (CH_2Cl_2); λ_{max}(nm), ϵ(M^{-1} cm^{-1}): 400(sh), 8370; 536, 8950; 700-(sh), 4100. MS(EI): m/z = 1027 [M^+, 100%].

Complex VL^{P}_2 (3). Yield: 0.37 g (68%). Anal. Calcd for $C_{68}H_{90}P_2O_4V$ (1084.35 g/mol): C, 75.32; H, 8.37; P, 5.71; V, 4.70. Found: C, 74.5; H, 8.5; P, 4.6; V, 4.8. IR (cm^{-1}): 3450(br), 2956−2868(s), 1425(s), 1241(s), 1105, 832, 744, 552. Absorption spectrum (CH_2Cl_2); λ_{max}(nm), ϵ(M^{-1} cm^{-1}): 436, 18560; 562, 12130; 700-(sh), 5930. MS(EI): m/z = 1083 [M^+, 100%].

Complex VL^{PO}_2 (4). Yield: 0.25 g (45%). Anal. Calcd for $C_{68}H_{90}P_2O_6V$ (1116.35 g/mol): C, 73.16; H, 8.13; P, 5.55; V, 4.56. Found: C, 72.7; H, 7.7; P, 5.9; V, 4.6. IR (cm^{-1}): 3449(br), 2959−2868(s), 1423(s), 1253(s), 1118, 832, 748, 544. Absorption spectrum (CH_2Cl_2); λ_{max}(nm), ϵ(M^{-1} cm^{-1}): 375, 8280; 542, 10 110; 700-(sh), 4510. MS(EI): m/z = 1115 [M^+, 100%].

Alternative Method for Synthesis of VL^{S}_2 (1) and VL^{Se}_2 (2). To a degassed CH_3CN (50 mL) solution of the ligand (1 mmol), $VOSO_4$ or $VO(acac)_2$ (0.5 mmol) was added. The resulting green solution was treated with 0.5 mL of Et_3N and refluxed under argon for $^1/_2$ h to produce a brownish violet solution. After being cooled to room temperature, the solution was kept under a slow sweep of argon where a brown microcrystalline compound was isolated in 50−55% yield depending upon the salt used.

Complex [$VO(L^{PO})(HL^{PO})$] (5). To a degassed hot CH_3CN solution (25 mL) of the ligand (0.5 mmol, 0.27 g), $VO(O^iPr)_3$ (0.25 mmol, 0.06 mL) was added. The colorless solution immediately turned blue-violet. After being cooled to room temperature, a crystalline violet complex was isolated, which was separated by filtration, washed with CH_3CN, and dried. Single crystals were grown from a solvent mixture of CH_2Cl_2 and CH_3CN (1:1). Yield: 0.21 g (74%). Anal. Calcd for $C_{68}H_{91}P_2O_7V$ (1133.36 g/mol): C, 72.05; H, 8.10; V, 4.50. Found: C, 71.3; H, 8.2; V, 3.9. IR (cm^{-1}): 3445(br), 2960−2868(s), 1431(s), 1223(s), 1254, 1121, 957, 841, 750, 552. Absorption spectrum (CH_2Cl_2); λ_{max} (nm), ϵ ($M^{-1}cm^{-1}$): 395, 5750; 537, 7120; 721, 3400. MS (EI): m/z = 1133 [M^+, 56%], 534 [H_2L^{PO}, 100%].

An alternative method. Complex VL^{P}_2, **3** was dissolved in CH_2Cl_2 and CH_3CN was layered over that. This solution, after being kept in air for 2 days, yielded a violet crystalline solid.

Complex [$(VO)_2(L^{Se})_2(\mu$-$OH)_2$] (6). To a hot CH_3CN solution (25 mL) of the ligand (1 mmol, 0.49 g), $VO(O^iPr)_3$ (1 mmol, 0.24 mL) was added. The colorless solution immediately turned blue-violet. After being cooled to room temperature, a crystalline violet complex resulted within 1 h, which was separated by filtration, washed with CH_3CN, and dried. Single crystals were grown from a solvent mixture of CH_2Cl_2 and CH_3CN (1:1). Yield: 0.30 g (52%). Anal. Calcd for $C_{56}H_{82}Se_2O_8V_2$ (1143.07 g/mol): C, 58.84; H, 7.23; V, 8.91. Found: C, 58.3; H, 7.0; V, 8.7. IR (cm^{-1}): 3443(br), 2958−2867(s), 1420(s), 1280(s), 1252, 1093, 992(s), 856, 757, 577. Absorption spectrum (CH_2Cl_2); λ_{max} (nm), ϵ ($M^{-1}cm^{-1}$): 511, 15120; 788, 8520. MS (EI): m/z = 1027 [decomposition product at high temperature, VL^{Se}_2].

Acknowledgment. Skillful technical assistance of Mrs. H. Schucht is thankfully acknowledged. We thank Andreas Göbels for skillful technical assistance with the MCD measurements. Useful discussions with Professor Thomas Brunold and Dr. Ralph Schenker (University of Wisconsin, Madison, WI) on the correction of MCD data are gratefully acknowledged. We are grateful to the German Research Council (DFG) for financial support (project: Priority Program Ch 111/2-2). F.N. and L.D.S. gratefully acknowledge financial support within the priority program of the DFG (Molecular Magnetism).

Supporting Information Available: X-ray crystallographic data in CIF format. This information is available free of charge on the Internet at http://pubs.acs.org.

IC040052F